2011

Advanced Semiconductor dosimetry in radiation therapy

Anatoly B. Rosenfeld
University of Wollongong, anatoly@uow.edu.au

Advanced Semiconductor dosimetry in radiation therapy

Abstract

Modern radiation therapy is very conformal, resulting in a complexity of delivery that leads to many small radiation fields with steep dose gradients, increasing error probability. Quality assurance in delivery of such radiation fields is paramount and requires real time and high spatial resolution dosimetry. Semiconductor radiation detectors due to their small size, ability to operate in passive and active modes and easy real time multichannel readout satisfy many aspects of in vivo and in a phantom quality assurance in modern radiation therapy. Update on the recent developments and improvements in semiconductor radiation detectors and their application for quality assurance in radiation therapy, based mostly on the developments at the Centre for Medical Radiation Physics (CMRP), University of Wollongong, is presented.

Keywords

radiation, therapy, advanced, semiconductor, dosimetry

Disciplines

Engineering | Science and Technology Studies

Publication Details

Rosenfeld, A. B. (2011). Advanced Semiconductor dosimetry in radiation therapy. In A. Rozenfeld (Eds.), Concepts and trends in medical radiation dosimetry (pp. 48-74). Melville, N.Y: American Institute of Physics.

Advanced Semiconductor Dosimetry in Radiation Therapy

Anatoly B. Rosenfeld

Centre for Medical Radiation Physics, University of Wollongong, Wollongong NSW 2522, Australia

Abstract. Modern radiation therapy is very conformal, resulting in a complexity of delivery that leads to many small radiation fields with steep dose gradients, increasing error probability. Quality assurance in delivery of such radiation fields is paramount and requires real time and high spatial resolution dosimetry. Semiconductor radiation detectors due to their small size, ability to operate in passive and active modes and easy real time multichannel readout satisfy many aspects of in vivo and in a phantom quality assurance in modern radiation therapy. Update on the recent developments and improvements in semiconductor radiation detectors and their application for quality assurance in radiation therapy, based mostly on the developments at the Centre for Medical Radiation Physics (CMRP), University of Wollongong, is presented.

Keywords: Dosimetry, radiation, LINAC, proton therapy, diode, MOSFET, quality assurance
PACS: 87.53Bn, 87.53Jw, 87.53Kn, 87.53Ly,87.55D, 87.55Qr

INTRODUCTION

Semiconductor detectors can be applied to all fields of radiation medicine, nuclear medicine, radiology and radiation therapy. Recently medical imaging technology has benefitted from the application of semiconductor based instrumentation developed for High Energy Physics (HEP), such as experiments on the Large Hadron Collider (LHC) at CERN. Silicon pixilated detectors, strip detectors and silicon photomultipliers (SiPM) now compete effectively with traditional photomultipliers. These devices are used in SPECT, PET, CT, intra-operative imaging probes and digital mammography. With the ongoing development of semiconductor radiation detectors and ASIC based electronic readout systems, semiconductor based instrumentation for radiation therapy dosimetry is advancing.

This paper will provide an overview of semiconductor radiation detectors for radiation therapy applications, including approaches to radiotherapy dosimetry currently under development or in the test phase. Semiconductor detectors are well suited to radiation therapy for absorbed dose, dose equivalent and radiobiological efficiency (RBE) measurements due to their small size, allowing for excellent spatial resolution, and the potential for real time read out. Previous work on nuclear spectroscopy with silicon detectors has translated to silicon microdosimetry and its application to dosimetry in neutron therapy, proton therapy and recently, new approaches in mini-dosimetry for brachytherapy.

Another class of semiconductor radiation detectors are based on the measurement of the change in the electrical characteristics of the semiconductor due to the introduction of radiation defects or ionization of dielectric layers in the device. This kind of detector is suitable for integral dosimetry. One such device is the Metal Oxide Semiconductor Field Effect Transistor (MOSFET). This detector has found wide application in conventional radiotherapy and recently for synchrotron microbeam radiation therapy (MRT) dosimetry where an excellent spatial resolution of the order of a micron or less has been obtained in real time, providing a unique contribution to MRT dosimetry.

PIN diodes have been used extensively for conventional photon and charged particle dosimetry via read out in ionization mode. While this is the most common mode of operation for PIN diode dosimetry, the diodes can be used in both radiation damage and ionization mode simultaneously to measure real time gamma and neutron, or neutron and proton dose components in mixed fields, such as fast neutron therapy and proton therapy respectively. The advantage being both measurements can be made with the single miniature detector.

Through many years of development and application, dosimetry with silicon radiation detectors has proven to be competitive with film dosimetry in regard to spatial resolution, and competitive with dosimetry using array ionization chambers in regard to two dimentional real time dosimetry. Rapidly developing silicon nanotechnology is

proving promising to the area of microdosimetry with silicon microdosimeters able to substitute the bulky Tissue Equivalent Proportional Counters (TEPC) microdosimeters. This is opening a new era of radiobiological quality assurance in radiotherapy.

The purpose of this paper is to provide an update on the recent developments and improvements in semiconductor radiation detectors and their application for quality assurance (QA) in radiation therapy, based mostly on the developments at the Centre for Medical Radiation Physics (CMRP), University of Wollongong, Australia. As well as providing a neat overview, the aim of this paper is to draw attention to the further opportunities that exist for silicon radiation detectors in radiotherapy. This paper is a logical extension of previous manuscripts on semiconductor dosimetry in radiation therapy presented at the Solid State Dosimetry (SSD) Summer Schools in Athens and Yale University [1,2] and should be read in conjunction with these two manuscripts.

INTEGRAL DIODE SEMICONDUCTOR DOSIMETRY IN RADIATION THERAPY

Conventional radiation therapy involves treating the tumor volume with either photons or electrons produced using medical LINACs or, as in brachytherapy, radio-isotopic sources. The accuracy required in delivering the dose to the target is usually within 2-3% [3]. Modern radiation therapy techniques, such as Intensity Modulated Radiation Therapy (IMRT), involve 'painting' the tumor volume with photons to provide a highly conformal dose with steep dose gradients. For such treatments a high spatial resolution is required for phantom dosimetry studies. Another challenging task in radiation therapy dosimetry is verifying the skin dose in breast, and head and neck treatments. Verification requires dosimetry at the depth of the epithelial layer of skin, i.e. about 0.07-1 mm, this limits the choice of detector suitable for such a measurement as packaging becomes a key issue. Real time dose verification for image guided radiotherapy (IGRT) is another important area that needs to be addressed to establish the appropriate QA. Semiconductor dosimeters are well suited to address these areas due to the following advantages they possess:

- A much higher sensitivity compared to an ionization chamber (IC) of the same volume (18000 times increase) due to a higher density and a smaller ionization energy compared to gas.
- A small dosimetric volume that satisfies the Bragg-Gray cavity theory in most practical circumstances, leading to high spatial resolution and the ability to place the detector within a confined space in the body and/or phantom.
- The possibility to operate the detector in passive mode (similar to TLDs) or on-line active mode (similar to ICs).

The three main semiconductor detectors to be considered in this section are silicon diodes, MOSFET detectors and diamond detectors. The first two detectors have the advantage that the silicon to water mass collision stopping power ratio is almost energy independent in the MV range typical of conventional photon and electron therapy. This leads to near tissue equivalency of the detector for MV radiation therapy dosimetry applications. A further advantage of using a silicon based detectors is that for very small sensitive volumes, such as the MOSFET detector (thickness <1μm), and for particular medical radiation sources, the Bragg-Gray cavity theory is satisfied down to photon sources of energy just tens of keV, making these detectors useful down to the KV range of photon dosimetry. When the range of the secondary electrons is less than the size of the dosimetric sensitive volume, the mass absorption coefficient ratio can become important, resulting in energy response of the dosimeters. Diamond detectors have the inherent advantage that the Z of diamond is 6, nearly matching the Z of muscle (7.2), leading to excellent tissue equivalency of the detector.

Most radiation semiconductor detectors are p-n junctions. p-n junction theory is well known and can be found in [4]. An advantage of the p-n junction is the inbuilt electrical field that exists at the boundary between the p-type and n-type silicon regions . The charge produced by ionizing radiation within the bulk of the material can be collected from this region through the diffusion of ionized electrons and holes to the junction. This diffusion into the inbuilt electric field at the junction is the basis of passive mode operation of a P-I-N diode (i.e. no externally applied bias). The diode can be used as a dosimeter of ionizing radiation where the amount of charge collected is determined by the diffusion length of the minority charge carriers and/or the base length of the detector. Taking into account the energy required for the production of e-h (electron-hole) pairs in silicon is 3.6 eV, it is possible to show that the number of electron-hole pairs generated in silicon per cGy per cm^3 is constant for silicon and equal to $4.2x10^{13}$ pairs/cGycm^3. The current induced in the diode is proportional to the dose rate. Integration of the current gives the charge deposited which is proportional to the absorbed dose in silicon.

Understanding the physics behind the response of a diode in current mode is complicated and can be affected by dose rate, temperature, radiation defects and depends on the initial Si material and radiation treatment before use.

Changing the dose rate of ionizing radiation affects the injection level and recombination properties of charge carriers in the base of the diode. Long term irradiation of the diode during use, either in phantom or in vivo, can lead to the accumulation of radiation defects and reduce the diffusion length of the charge carriers, ultimately reducing the sensitivity of the detector. A change in the temperature affects the level of recombination in the diode and ultimately the response. These performance affecting factors make the development of a good dosimetric diode quite a complicated task. Before any diode can be used, detailed characterization is required.

Many different approaches have been implemented to reduce the dose rate dependence of the diode: a reduction in the resistivity of the diode base, application of p-Si rather than n-Si, and pre-irradiation of the diode. In radiation therapy it is necessary to take into account that while the average dose rate during treatment is only about 200-400 cGy/min. The actual dose rate is of the order of 10^4 cGy/s due to the pulsed delivery from the medical LINAC. A more detailed analysis concerning the dose rate effects due to: initial parameters of the diode Si, pre-irradiation and fabrication technology can be found in [4,5].

The loss of sensitivity of a dosimetric diode due to radiation degradation depends on the energy of the incident radiation from the medical LINAC. The greater the energy the greater the degradation. To reduce this affect for p-type diodes, the diodes can be irradiated prior to use or by reducing the initial life time of the charge carriers by doping the base of the diode. The typical loss in sensitivity of a commercial diode is 20-25% for an accumulated dose roughly greater than 10 kGy on electron and photon beams [6].

The variation in response of a diode due to temperature was observed to be in the range 0.02-0.28% per ^{0}C for Scanditronics, Sun Nuclear and PTW diodes as reported in [5,7,8]. The variation depends on the prehistory of the diode and the initial material. This instability can affect the accuracy of the dosimetry, especially when the diode is placed on the body of the patient [8].

Diodes play an important role in radiation dosimetry. Single diodes can achieve a spatial resolution of about 1-2mm and are well used in relative dosimetry for depth dose verification, beam profiling, as well as in vivo entrance and exit dose measurements. Dosimetry systems based on an array of single diodes have been built for 2D, and recently 3D, dose QA in IMRT and Volumetric Modulated Arc Therapy (VMAT). 2D diode arrays, for example MapCHECK has 445 Si diodes with 10 mm pitch, are useful for 2D relative dose mapping in a particular plane of the phantom perpendicular to central axis of each beam [9, 10, 11] and have proven themselves useful in IMRT QA. The pitch between diodes, usually 10mm outside and 5mm in the central part of the diode array, limits their spatial resolution in steep dose gradients, where often only one or two measurement points will be in the 20–80% penumbra region [10].

Recently, several diode based dosimetry systems were developed for 3D dose plan verification in IMRT and VMAT. These devices have been fully characterized. The ScandiDos Delta4 (ScandiDose AB, Sweden) has bi-planar orthogonal diode array planes with a total of 1069 p-Si diodes contained in a cylindrical phantom. This system allowed accurate QA of a complicated 3D dose plan delivery and provided absolute dosimetry on line [12,13,14]. Another system has been developed and tested. This ArcCHECK system has an isotropic arrangement of 124 diodes embedded in a cylindrical phantom (ArcCHECK, Sun Nuclear Corporation, Melbourne, FL) [15]. Both systems take into account temperature instability corrections of the diode, along with their angular and relative response variation via a quite complicated algorithm implemented to convert the real time response of the diode. This system has proven useful for pre treatment QA in IMRT. Details of the clinical applications of Delta4 can be found in this book [V.Feygelman et al.]

In spite of their small size most of commercial diodes cannot be used for surface dosimetry. This is due to the presence of packaging leading to a build up region that changes the depth of measurement. Fig 1 shows 3 typical dosimetric diodes, the packaging of each leads to a different build up characteristics when used in radiation therapy. Usually for 1-4 MeV photons the build up material is aluminium or copper, for 4-6 MeV photons brass is an option, and for 12-25 MeV photons tungsten is used.

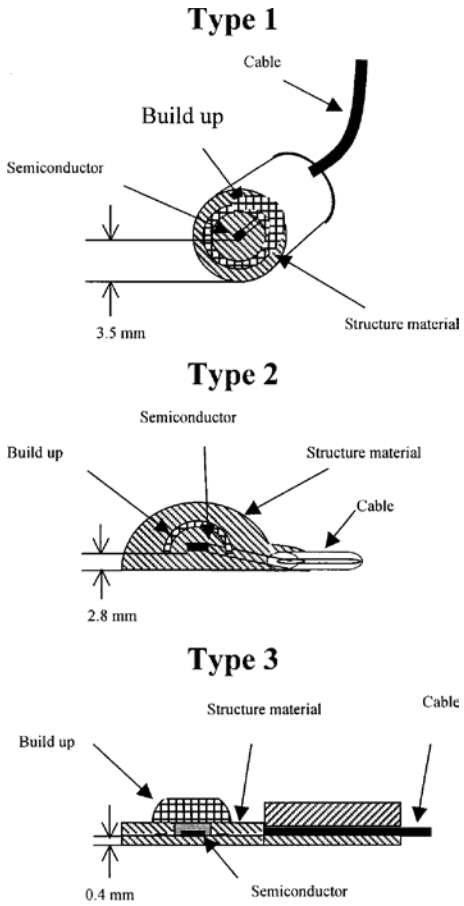

FIGURE 1 . Typical packaging of dosimetric diodes used in conventional therapy with different X-ray energies. (Reproduced from [16]).

The diodes are intrinsically asymmetrical due to the sensitive region of each diode being surrounded by non uniform passive layers of silicon. These layers attenuate photons and produce electron backscattering with different characteristics than water. Additionally, the packaging of the diodes essentially determines their angular response; for more uniform angular response, high z-elements should be avoided in the diode packaging [17].

Single diodes and diode array detectors are one of the major and most convenient QA tools for relative and absolute dosimetry in radiation therapy. They have some limitations when high spatial resolution is required, and in particular the packaging and size of their sensitive volume can be an issue for skin dosimetry.

.

HIGH SPATIAL RESOLUTION SEMICONDUCTOR DOSIMETRY

High Spatial Resolution Dosimetry Using Diode Structures

For high spatial resolution dosimetry, arrays of diode structures fabricated on silicon wafers like pixel or strip detectors, in addition to single diodes and single diode arrays, have been found very useful. They are convenient for multichannel readout using specially developed VLSI Application Specific Integrated Circuits (ASICS).

In Europe, the MAESTRO project (MAESTRO, 2008) proposed the development of pixelated Si detectors for high spatial resolution medical radiation dosimetry. The detector involved is a monolithic silicon segmented module [18]. Each pixel comprises of a p-n junction surrounded by a guard-ring structure implanted on an epitaxial 50 μm thick p-type Si layer grown on a Czochralski substrate. The sensitive area of each pixel is 2×2 mm^2 with a 3 mm

pitch. The first 441 pixels, 6.29x6.29 cm^2 silicon module has been produced. This sensor has been connected to discrete readout electronics performing current integration and has been tested with satisfactory results. In the final configuration, nine silicon modules will be assembled together to cover an area close to 20x20 cm^2 with 3969 channels with ASIC readout electronics. This system has been shown to offer better resolution than most commercial 2D discrete diodes.

The silicon strip detector is another position sensitive detector which is being developed by various groups for high spatial resolution medical radiation dosimetry. It is based on a planar array of p-n junction strips and widely used in high energy physics tracking detectors. Silicon strip detectors were used to characterize a Sr-90 intravascular brachytherapy source in terms of dose-depth curves in a tissue equivalent material, as well as the homogeneity of the source activity [19]. Another group has developed a 128 channel strip detector, the area of each strip being 0.25 × 0.25 mm^2 and pitch 0.3 mm, for stereotactic radiotherapy dosimetric verification [20]. Their work shows good agreement with a diamond detector for penumbra measurement applications [20,21].

Dose Magnifying Glass

Since 2003, the CMRP has been developing the concept of a high spatial resolution silicon dosimetry system with a large dynamic range (of the order of 10^3) for applications on medical linacs. The system is based on silicon strip detector technology. The Dose Magnifying Glass (DMG) is an array of 128 phosphor implanted n+ strips on a p-type silicon wafer (Fig 2). The sensitive area is defined by the dimensions of the n+ strip. DMGs with two different sensitive areas were designed: 0.02 × 5 mm^2 and 0.02 × 2 mm^2. The thickness of the Si wafers is 375 μm and the pitch of the strips is 200 μm. Boron implanted p+ layers isolate the strips and prevent shorting of the n+ strips due to the ionizing radiation induced positive build up charge in the SiO^2. Aluminum was evaporated on top of n+ areas, connected to Ni leads fanning out to two 68 channels connectors. The detector can be used in passive mode or biased mode and read out was carried out with the detector configured as a planar detector with a common p+ electrode on the same side as the n+ strips. Two types of device were produced, one with a resistivity of 5 kOhm·cm float zone silicon and the other with resistivity of 10 Ohm·cm Czochralski silicon.

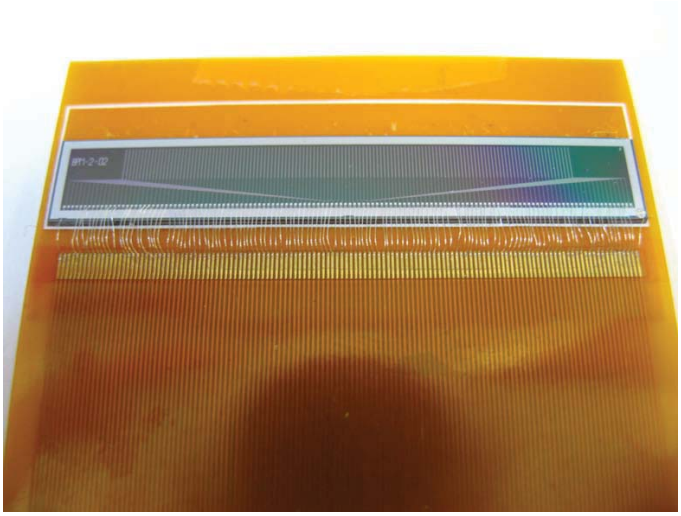

FIGURE 2. DMG mounted on 0.12 mm thick kapton.

Tera VLSI ASIC Chip

The data acquisition (DAQ) system is an important issue in high spatial resolution real time dosimetry due to the requirements for simultaneous readout of multiple channels (sensors). The readout electronics for the DMG uses two 64 channel TERA VLSI ASIC chips that allow instantaneous readout of multiple channels. The TERA chip was designed by the Istituto Nazionale di Fisica Nucleare (INFN) - Torino Division and University of Torino microelectronics group working on the readout of pixelated ionization or strip chambers for hadron therapy (http://totlxl.to.infn.it/NewSite/vlsi_chip.html, [22]). The ASIC is a current to frequency converter, followed by a

16-bit counter. It has a dynamic range of $> 10^5$ and is capable of measuring currents from a few pA to a few μA with a nonlinearity of less than 1%. The current to frequency conversion is based on the recycling integrator principle. The current is integrated via an operational transconductance amplifier (OTA). When the OTA output reaches a threshold level, the charge subtraction circuit is activated and the integrated current or charge is reduced by a fixed quantum charge, at the same time a pulse is issued to the counter. This charge subtraction method is far superior to the traditional resetting of the integrating capacitor, since the input current continues to integrate even during the charge subtraction. Hence, there is no dead time [23,24].

Various versions of the TERA family of ASICSs have been successfully implemented in the "Magic Cube ionization chambers in hadron therapy [25-27] and in the gas ionization chamber based 2D planar array IMRT MatriXX and StarTrack (IBA Group, http://scanditronix-wellhofer.com/2D-verification.1458.0.html).

DMG Detector Characteristics

Silicon detectors have some disadvantages due to their dose rate dependence, angular dependence, energy dependence, and radiation damage susceptibility. However, with careful characterization, they are useful for relative dosimetric purposes.

Similar to all Si detectors, the DMG is energy dependent and therefore sensitive to changes in the beam spectrum. The energy response of the DMG was studied for the energy range of 50kV to 10 MV nominal energies (corresponding to 26.8 keV – 2.97 MeV equivalent photon energies) [28]. The detector showed an enhanced response, up to six times, at lower photon energies with the maximum dose response at 75 kV nominal photon energy due to the increased photoelectric effect cross-section in silicon at low energies [29].

Due to the planer detector design as well as the ceramic substrate detector mounting, the maximum angular dependence of the DMG was 28.1% when the beam was incident parallel to the detector plane [28]. The 2nd generation of DMG, which was mounted on a 0.12 mm Kapton substrate, was able to improve the angular dependence by 12.8%.

The dose rate dependence of the DMG is affected by the silicon resistivity and the pre irradiation conditions, much like a single silicon diode. The dose rate dependence can be reduced to 2% by using p-Si diodes made from low resistivity silicon, and by pre-irradiating the diodes to reduce the initial life time of charge carriers in the base material [5]. For the dose rate range of 200 – 840 cGy/min, the dose rate variation was < 5% for the unirradiated low resistivity device while for the pre irradiated device (irradiation with 15 kGy of 1 MeV electrons), the variation in dose rate response for the dose rate range of 80 – 600 cGy/min was < 2%.

The linearity of the DMG for the dose range of 3.89 cGy to 311.05 cGy was excellent, while the depth dose measurement of a 6 MV photon beam shows good agreement with an ion chamber (within 0.8%) at all points up to 20 cm depth [28]

Application in Intensity Modulated Radiation Therapy

Intensity modulated radiation therapy (IMRT) is a complex mode of radiation delivery. It utilizes a multileaf collimator (MLC) to modulate the radiation beam to achieve dose escalation to the tumor while sparing the critical organs close to the irradiated target. IMRT plans tend to produce steep dose fall off regions at the interface of the target and organ-at-risk. The complexity of the IMRT delivery demands a far more rigorous quality assurance (QA) verification. In many facilities, patient based QA checks were carried out using ionization chambers for point dose measurements along with 2D or 3D diode or ion chamber arrays such as MapCHECK, IMRT MatriXX (IBA, http://scanditronix-wellhofer.com/2D-verification.1458.0.html) or Delta4 for fluence verification. These diode arrays are limited by their spatial resolution in high dose gradient regions [11,30]. IMRT dosimetric verification using the DMG is detailed in [28]. The benefit of 0.2 mm spatial resolution and the high temporal resolution measurement of the DMG was evident as it was able to capture the real time dose modulation for the IMRT delivery. Figs 3 and 4 show the IMRT dose profiles for different gantry angles and the cumulative dose growth as measured by the DMG.

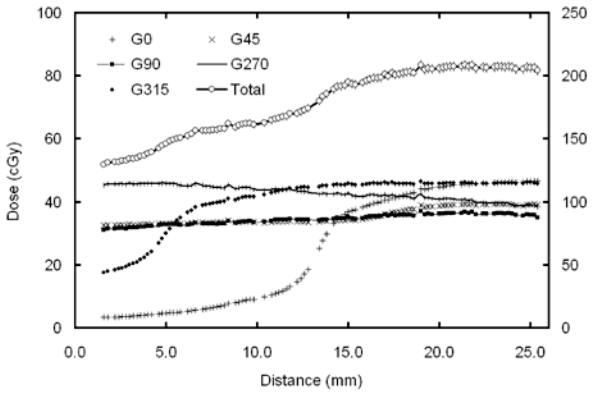

FIGURE 3. IMRT dose measurement for different gantry angles. (Reproduced from [28]) .

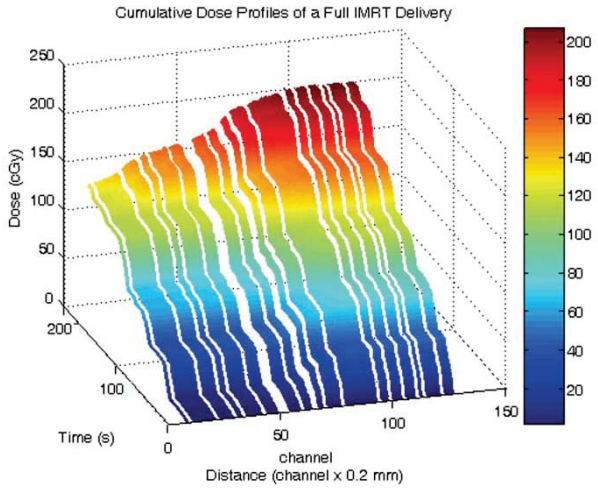

FIGURE 4. Cumulative dose profile of an IMRT delivery. (Reproduced from [28]).

Application in stereotactic radiosurgery/radiotherapy (SRS/SRT)

Stereotactic radiosurgery (SRS) is the use of radiation to ablate a small lesion (usually < 4 cm in diameter) in the body. The treatment is normally delivered in a single large dose, resembling a surgery, hence the name. In some cases, the treatment is delivered in several smaller fractions; this is usually called stereotactic radiotherapy (SRT). The delivery of this treatment requires the use of stereotactic frames for precise target localization. This treatment delivery requires a tight margin with sharp dose fall off [31]. Hence, its quality assurance QA verification demands high geometric precision and accuracy. The challenge in SRT/SRS dosimetry is verifying the dose delivery with a trusted QA procedure in such a small field size. Dosimetry in small fields is susceptible to the problem of lateral electronic disequilibrium where more secondary electrons are generated by photons within the fields and scattered outwards, while less electrons are scattered into the field. On the other hand, the use of ion chambers or diodes with an active area that is comparable to the field size being measured (< 10mm) raises the issue of detector volume averaging that reduces the dose measured at the center of the beam, while artificially broadening the penumbra width. The clinical significance of this would be a systematic over-irradiation of the organ-at-risk arising from attempts to ensure sufficient PTV coverage during planning [20,32]. Insufficient spatial resolution of the detector that was used to collect the beam data during commissioning of the IMRT planning tool will produce error in the beam modeling of the treatment planning system, resulting in local discrepancies of > 10% between calculated cross profiles and profiles measured with films [33]. The authors also showed that the absolute dose difference was reduced to < 2% by simply using a detector with a smaller cross section, such as a 0.015 cm^3 pin point ion chamber. Common techniques for SRS delivery are x-ray and gamma knife. For x-ray based SRS treatments, the treatments

are carried out using a linear accelerator which delivers radiation to the target at iso-center with various non co-planar arcs. However, in order to produce narrow beams for the small targets, tertiary collimators such as the micro multileaf collimator or cones are often used. DMG with the sensitive area of 0.02 × 2 mm^2 is particularly useful for SRS QA and dosimetry. The DMG mounted on the end of a 0.12 mm kapton pigtail encapsulated in a solid water holder was used in conjunction with a custom made solid water head phantom. The phantom was screwed onto the commercial SRS couch mounting frame (fig. 5) [34]. This allows the DMG to measure non coplanar SRS treatment deliveries. One of the SRS QA procedures required prior to SRS delivery is the measurement of the center of rotation (COR) and position offset of the linac. The 0.2 mm spatial resolution capability of the DMG is comparable with the resolution of film dosimetry but with the added advantage of real time electronic readout. The COR of the linac gantry was determined from the center of the beam profiles obtained from the 0° and 180° gantry rotation. The COR offset is defined as half the difference between the x-coordinates of the two mid points of the beam profiles (fig. 6). The determination of the collimator and couch rotation was also determined in this manner.

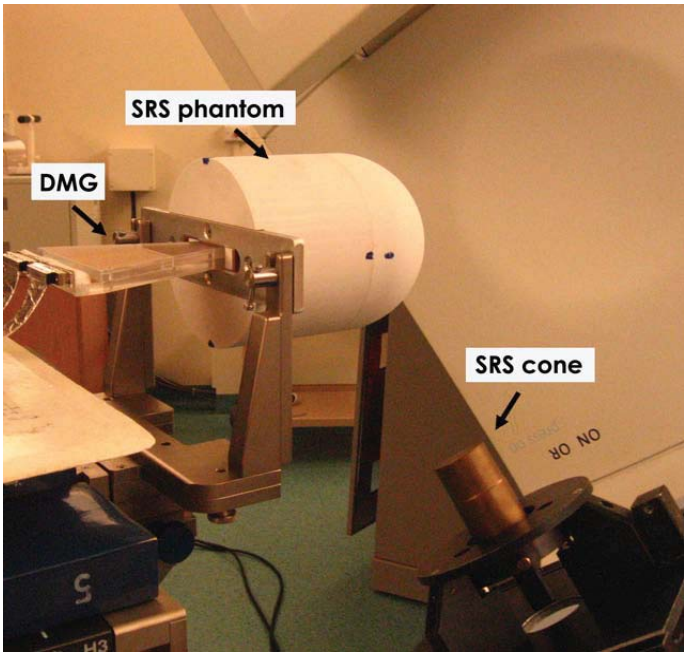

FIGURE 5. Experiment setup of DMG mounted in custom made SRS phantom for SRS treatment verification.

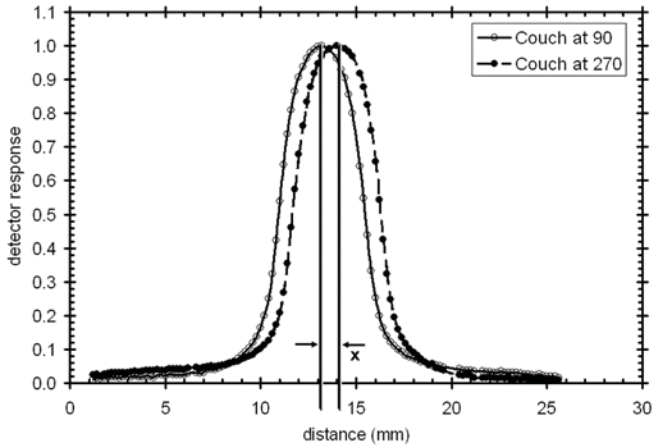

FIGURE 6. DMG used to measure the center of rotation offset. (Reproduced from [34]).

Application in helical tomotherapy

Helical tomotherapy is a radiotherapy treatment technique that is very different from the conventional linac. It resembles a diagnostic computed tomography (CT) machine in that it has a rotating gantry and it delivers radiation as the patient is translated through its bore. Similar to CT machine, it has an integrated imaging system comprising of 738 xenon filled ion chamber MVCT detectors sitting opposite the 6 MV linac, allowing the integration of image guidance and intensity modulated radiation therapy in a single system. Another feature that contrasted the helical tomotherapy with conventional linac is that the helical tomotherapy employs a binary multileaf collimator (MLC) instead of the conventional field shaping multileaf collimator to modulate the radiation [35,36]. The binary MLC is a 64-leaf tungsten inter-digitated across the field. Modulation of the radiation is achieved by temporal modulation of the binary MLC as the linac rotates around within the gantry housing. This unique mechanism for dose modulation results in a unique dosimetric characteristic that is not present in a conventional IMRT delivery. New quality assurance procedures were devised to ensure the accuracy of the helical tomotherapy delivery [36-39]. Examples of helical tomotherapy specific QA procedures are: the MLC and gantry misalignment test, and leaf latency measurements. The MLC and gantry misalignment test is usually carried out during machine commissioning and after a new MLC bank is installed to ensure that the MLC misalignment is within the tolerance limit of ± 1 mm. The helical tomotherapy binary MLC can have only two states, open or closed. Due to the physical limitation of the mechanical and pneumatic system, a finite time is required for the leaf to change from a closed state to an open state and vice versa. This is known as the leaf latency.

The use of the on board CT detector provides a convenient way of performing many of these QA procedures. Besides that, film is also one of the common dosimeters used for QA measurements. The DMG was proposed as an independent tool for performing some of the common QA procedures of helical tomotherapy [40]. Figure 7 shows the measurement of MLC misalignment using the DMG. For this measurement, the two central leaves (32 and 33) were opened and closed sequentially at a gantry angle of 0°. The gantry was then rotated to an angle of 180° and the same exposure was made. The double peak profile is the result of the tongue and grooves – penumbral effect of delivering the radiation by sequential opening and closing of the two adjacent leaves [39]. The MLC offset error was determined as half the distance between the mid points of the two profiles. The difference between the EDR2 film and DMG measurement was 0.16 mm, within the uncertainty of the measurements. Fig. 8 shows the leaf latency measurement of a tomotherapy leaf for the projection time of 50 ms to 303 ms. The leaf open time was programmed to open for a fraction of time and this is expressed as a percentage of the maximum projection time.

The DMG was shown to be a suitable tool for providing machine independent QA checks in tomotherapy, with the capability to provide sub-millimeter resolution of any MLC misalignment and real time high temporal resolution measurements of leaf latency.

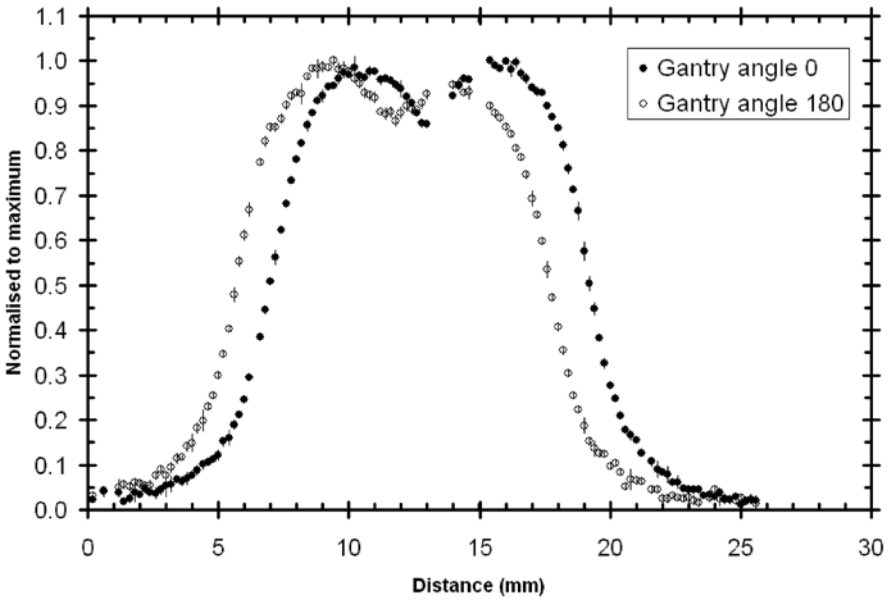

FIGURE 7. MLC misalignment measurement using DMG. (Courtesy J.Wong *et al* [40]).

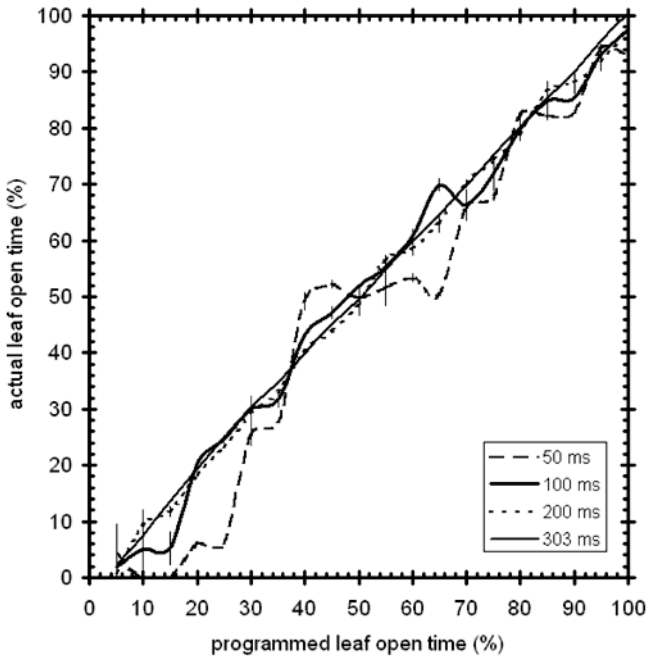

FIGURE 8. Helical tomotherapy leaf latency measurement for 50 ms, 100 ms, 200 ms and 303 ms projection. The leaf open time is expressed as percentage of the maximum leaf open time, i.e. a 50% of a 200 ms projection is 100 ms.(Courtesy J.Wong *et al*. [40])

MOSFET DOSIMETRY

The application of MOSFET detectors to radiation therapy dosimetry is relatively new in comparison to conventional diode detectors. Actually, the application of MOSFET detectors to dosimetry was originally proposed for monitoring of space radiation doses to predict integral dose effects for electronics on satellites [41].

The main idea behind the operation of the MOSFET detector is the changing of the threshold voltage, Vth, which is the voltage on the gate of the MOSFET relative to the source. The change in V_{th} is due to the buildup in charge produced by ionizing radiation in the gate oxide, mostly at a Si-SiO^2 interface. Fig. 9 shows the principal of operation of the MOSFET detector.

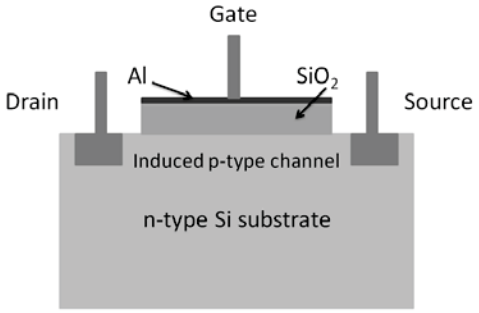

FIGURE 9. Schematic of an n-type MOSFET detector. Buildup charge in the gate oxide is produced by ionizing radiation.

Accumulated charge in the gate oxide is quite stable at room temperature. MOSFET detectors also exhibit only a small degree of fading (the deterioration of the signal over time), however, this depends on the oxide growing and annealing technology used during manufacturing. In these perspectives, the features of the MOSFET are similar to TLD detectors, allowing for readout of the MOSFET detector some time after irradiation with minimal deterioration of information. The sensitivity of the MOSFET detector is proportional to t_{ox}^2, where t_{ox} is the gate oxide thickness.

More detailed information on the fundamental physics and response of the MOSFET and RADFET detector to photon, electron and charged particle fields can be found in [42-45]. There are many advantages of MOSFET detectors in dosimetry applications, such as the extremely small size of the dosimetric volume (the gate oxide has a thickness of less than 1 micron, which is currently not feasible with other radiation detector technologies) dose rate independence, the possibility to compensate temperature instability of V_{th} by using a built in thermometer, which is the p-n junction as a part of the MOSFET, real time readout during treatment delivery in radiation therapy [46-48] and the possibility of sensitivity adjustment by alteration of the gate bias during irradiation [43, 49]. MOSFET detectors produced in the same batch show reproducible results, with a spread in sensitivity within 1% [48]. This property makes them attractive for disposable applications, utilizing a "one dose" principle [50].

All of the above mentioned advantages of the MOSFET detector make them useful for dosimetry in locations of strong electronic disequilibrium. Such sites include the surface of the body, or anatomical cavities, and in buildup regions of MV X-ray beams. Thus, MOSFETs are suitable for dosimetry measurements in fields exhibiting a steep dose gradient, where the volumetric effect experienced by ionization chambers results in unreliable measurements.

There are currently two MOSFET dosimetry systems offered on the commercial market. These are produced by Best Medical Canada Ltd. (Ottawa, Ontario, Canada) and Sicel Technologies (Morrisville, NC, USA) which produce the OneDose™ system. An extensive bibliography on clinical applications of commercial MOSFET dosimetry systems in diagnostic and therapeutic radiation fields can be found in [http://www.mosfet.ca/publications/index.htm]

The Centre for Medical Radiation Physics (CMRP), University of Wollongong, is a developer of clinical MOSFET dosimetry systems. The Centre has obtained extensive experience with MOSFET dosimetry applications in a range of different radiation oncology modalities including medical LINACs [51-55], brachytherapy [56,57], microbeam radiation therapy [46,58-61] and neutron therapy [62-64]. A summary of the advantages and challenges of MOSFET dosimetry in a range of radiation therapy modalities has been presented in [2]. In the current review article we would like to demonstrate the further progress and advantages of MOSFET dosimetry, and in particular the new MO*Skin*™ detectors developed at the CMRP. The new MO*Skin*™ detectors are capable of measuring skin doses, which ICRP 1975 recommends be measured at a depth of 0.07 mm [65].

Theoretically, the dose deposited at the surface (surface dose) and in the buildup region (entrance dose) of photon fields has two main contributors [66]. One is in-phantom scatter, due to photon interactions with the phantom material and subsequent generation of secondary electrons, which deposit energy along their path. The second is electron contamination, which derives from electrons produced outside the phantom striking the phantom surface, e.g. through photon interactions in the LINAC head.

In practice, in vivo surface dose measurements represent a significant technical challenge as the epidermal layer of the skin is only 0.07 mm thick, approximately, and the radiosensitive basal layer lies at this depth [65]. The challenge of skin dose monitoring exists in breast cancer treatments, head and neck IMRT delivery and on the surface of the rectum wall during prostate cancer treatment, among others.

Similar to diode detectors, the response of MOSFET detectors depends on packaging technology. Most manufacturers place the MOSFET chip on a KAPTON film or thin printed circuit board carrier to which the MOSFET is wire bonded. An epoxy bubble is then placed on the top of the MOSFET chip for protection. For the MOSFET from Best Medical, the chip is mounted on a KAPTON carrier and covered by approximately 1 mm of epoxy coating. The equivalent depth in water for TN MOSFET sensors is 0.8 mm and 1.8 mm for the flat-sided and round-sided dosimeters, respectively, on the epoxy bubble side. This corresponds to percentage depth doses of 35.6% and 56.1%, respectively, in relation to dose at D_{max} for a 10×10 cm^2 field of 6MV X-rays [67] instead of 16% when measured by Attix parallel plate IC. A similar packaging effect with a RADFET chip consisting of 0.2 mm printed circuit board carrier, covered with a 0.3 mm epoxy bulb (REM Oxford Ltd.), was observed in surface dose measurements in a hemi-cylindrical solid water breast phantom of 7.5 cm radius irradiated with 6 MV X-rays when compared with GaF Chromic film measurements [51].

The MO*Skin*™ detector utilizes different chip packaging technology. Here, the protective epoxy bubble is replaced by a thin polyamide film. The design is presented in Fig. 10.

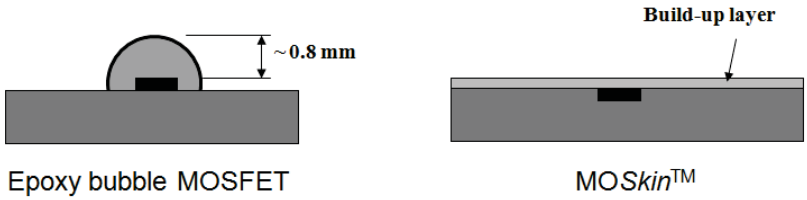

FFIGURE 10. Comparison of the packaging between a typical MOSFET detector (a), and a MO*Skin*™ detector (b).

The MO*Skin*™ detector utilizes "drop in" technology, where a buildup polyamide film with thin Al leads has a reproducible water equivalent depth (WED) of 0.07 mm. The film is used for both electrical connection of the MOSFET chip to the KAPTON pigtail and chip protection. In such a design, the MOSFET chip is embedded in a 0.35 mm thick KAPTON pigtail and protected from the environment with polyamide film on both sides. Fig 11 shows a MO*Skin*™ probe.

FIGURE 11. CMRP MO*Skin*™ probe. The pigtail is 40 cm in length, with drop in MO*Skin*™ detector at the end.

Fig. 12 shows a comparison of the response of the MO*Skin*™ detector placed "face up" on the surface of a solid water phantom (gate oxide facing the incident beam) irradiated with a 6 MV X-ray field from a medical LINAC.

Curves are shown for 10×10, 5×5 and 2.5×2.5 cm^2 field sizes and 100 cm focus-to-surface distance (FSD). Measured doses are presented relative to the dose at D_{max}. The three solid curves in Fig. 12 represent percentage depth dose (PDD) curves produced by Monte Carlo simulations at CMRP, and are presented on a semi-log scale. The response of the MO*Skin*™ detectors correspond to doses measured at a WED of 0.07 mm for all three radiation fields.

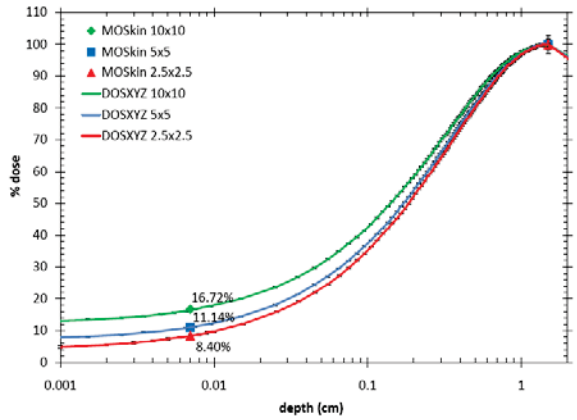

FIGURE 12. Response of the MO*Skin*™ dosimeters on the surface of a solid water phantom in comparison to Monte Carlo PDD simulations. This demonstrates that the WED of measurements with the MO*Skin*™ is 0.07mm.

Fig. 13 shows the change in V_{th} for six randomly selected MO*Skin*^{TM} detectors from the same batch following irradiation with up to 10 Gy [48]. The response of the six MO*Skin*^{TM} detectors was uniform over the 0-10 Gy dose range. For the MO*Skin*^{TM} detectors used in this study, the calibration factor (CF) was 2.64 mV/cGy and the response linear with $R^2 = 0.99994$. These measurements were performed under a +15V gate bias during irradiation, using a real-time computerized CMRP MOSFET reader.

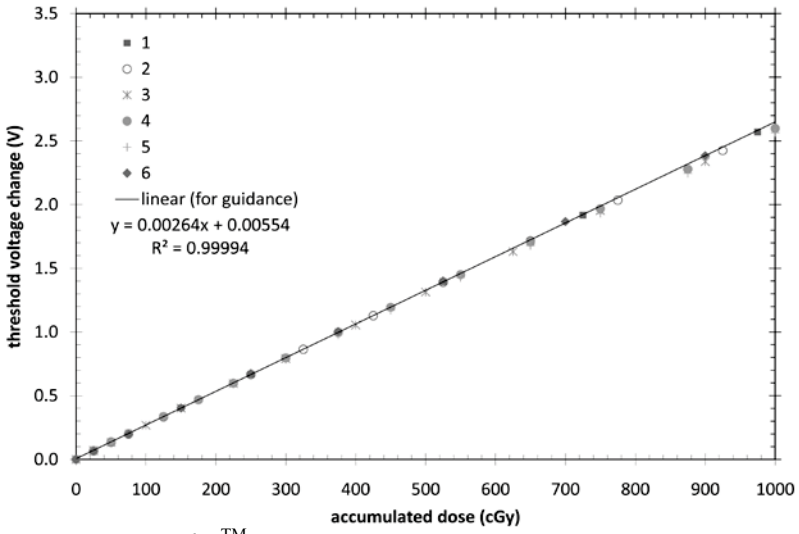

FIGURE 13. Change in V_{th} for six MO*Skin*^{TM} detectors for doses up to 10 Gy. A linear trend line has been fitted for guidance.

The linear response of the MO*Skin*^{TM} detectors makes them ideal for disposable applications, such as in vivo skin and surface dosimetry after each or several fractions of radiation delivery, at sites with electronic disequilibrium. Examples of the attractive applications of the MO*Skin*^{TM} include real-time dosimetry on the surface of the rectal wall during HDR brachytherapy and IMRT for prostate cancer and head and neck treatments.

A study was carried out to compare predicted and MO*Skin*^{TM} measured surface doses during IMRT delivery for a head and neck treatment [68]. A specially designed MO*Skin*^{TM} detector was placed on the interface between the oral plate and tongue during CT-simulation and treatment. The detectors were identified on the patient CT images and calculated point doses recorded during the treatment planning process. The measured doses were recorded in real-time during treatment delivery. Fig. 14 shows the Corvus (Best Nomos, Pittsburgh, PA, USA) IMRT treatment plan with the MO*Skin*^{TM} detector clearly identifiable on the sagittal CT images. Fig. 15 illustrates an example of the V_{th} change, measured in real-time over 30 seconds with readout each second. The figure shows a) integral dose mode and b) dose increment mode. This clearly demonstrates the ability of the MO*Skin*^{TM} to measure small dose increments (1-5) cGy and the pattern associated with MLC leaf motion during IMRT [69]. Results demonstrated that the individual patient variation of IMRT delivery to the tongue was less than 5% over the course of treatment, illustrating the in vivo application of the MO*Skin*^{TM} to dose verification.

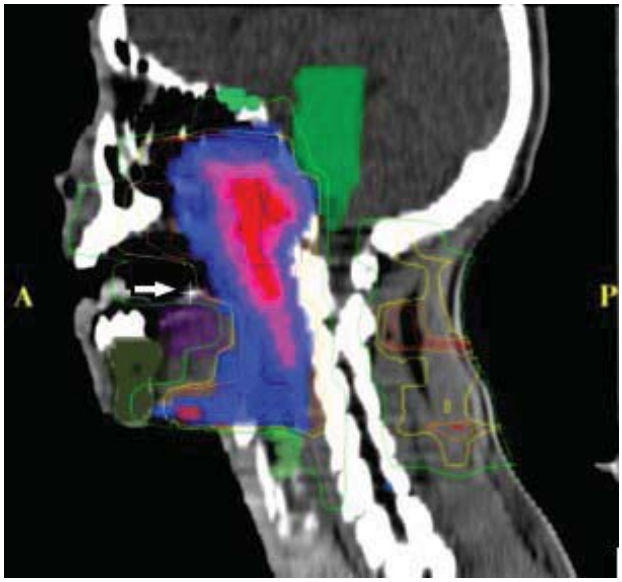

FIGURE 14. Example of Corvus IMRT treatment plan. The MO*Skin*™ detector can be identified on the patient CT images as shown by the white arrow.

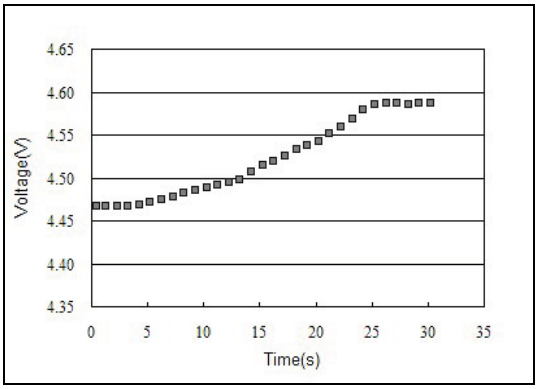

a)

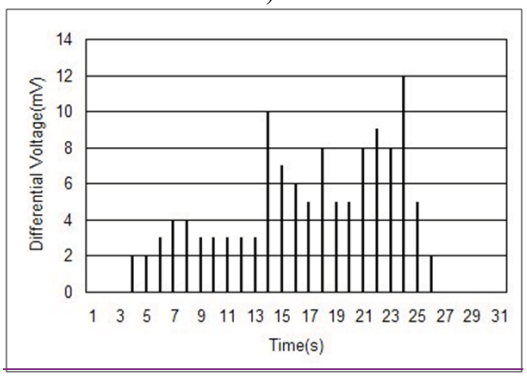

b)

FIGURE 15. A sample IMRT measurement of in vivo doses on the tongue during a single treatment fraction for nasopharyngeal carcinoma using real time MOSFET dosimetry system. a) accumulated dose variation; b) dose increment variation.

The CMRP MO*Skin*™ detectors were also applied to IMRT in vivo skin dosimetry for nasopharyngeal carcinoma (NPC) patients [47]. Several MO*Skin*™ detectors were placed on the head surface as radio-opaque markers during CT scanning. These MOSFETs were identified in the treatment planning system (TPS) and the

calculated doses delivered to the detectors recorded. The dose difference between the MO*Skin*™ measurements and TPS calculations was on the average of -7.2% ± 1.2%, ranging from -4.3% to -9.2%. This reveals that attention should be paid to the skin dose calculations in the TPS system which overestimated dose at these superficial sites. Other authors have reported similar results using film dosimetry [70], however the unique advantage of the MO*Skin*™ lies in its ability to provide real-time surface dosimetry.

The application of MO*Skin*™ detectors to HDR brachytherapy has also been investigated. A custom made phantom containing special catheters for Ir-192 source dwelling was created to simulate the treatment of NPC. Dosimetry measurements with the MO*Skin*™ demonstrated good agreement with a specially created CT based treatment QA plan [57]. The percentage deviations between the measured doses and the planned doses were below 5% for all the measurements at different orthogonal distances of the MO*Skin*™ from source train. The advantage of the MO*Skin*™ probe design in comparison with the epoxy bubble based MOSFET package was reflected in the reduced energy dependence of the MOSFET sensitivity with distance from the Ir-192 source. Changing the distance to the source from 1 to 5 cm resulted in a change in sensitivity of the MO*Skin*™ within 7% while a corresponding change of 24% was observed for a bubble based MOSFET (RADFET). This is associated with the dose enhancement due to the additional epoxy buildup, which has a higher atomic number than water [70].

MO*Skin*™ probes have been used to measure the dose from an Ir-192 HDR brachytherapy source along an empty air cavity in a phantom, simulating an empty rectum [71]. When placed along the wall of the empty rectal phantom, the dose measured by the MO*Skin*™ on the anterior rectal wall was 15.3% lower than the dose measured in a full rectal cavity at the same point. This was corroborated by the results obtained through a Monte Carlo GEANT4 simulation, showing that the dose deposited along the anterior rectal wall of the empty cavity was 16.2% lower than in a full cavity. This demonstrates the usefulness of MO*Skin*™ detectors for surface dosimetry on the rectal wall in HDR brachytherapy.

The response of the MO*Skin*™, as with all MOSFET detectors, is asymmetric by nature. This is due to the sensitive volume being located on a silicon slab, resulting in a non-uniform angular response. The design of the MO*Skin*™ probe mentioned above utilizes two MO*Skin*™ detectors in a face-to-face orientation, which has been dubbed the dual MO*Skin*™. This leads to a symmetrical structure because the sensitive volume of each MO*Skin*™ is sandwiched between two silicon substrates and covered with 0.14 mm WED polyamide films. The response of the dual MO*Skin*™ is the sum of responses of both detectors. It was demonstrated that the angular response of the dual MO*Skin*™ is flat within ± 2.5% for the azimuth axis and -2.5% and +4% for the polar axis [48].

The dual MO*Skin*™ was applied to point dosimetry on the anterior rectal wall in external beam radiotherapy, in conjunction with an endorectal balloon used for immobilization of the prostate (see Fig. 16). In vivo dosimetry of the rectal wall is an appealing method for verification of target and organ at risk (OAR) doses. An in vivo dosimeter placed on the anterior rectal wall would allow the clinician to measure the dose delivered to the section of the rectum receiving the highest dose. This is important, particularly for recent hypofractionation schedules, where high doses are delivered to the prostate and anterior rectal wall, and would be particularly useful in the context of the limitations of dose calculation algorithms at cavity interfaces. Additionally, accurate knowledge of the anterior rectal wall dose is necessary for correlation of delivered dose to rectal toxicity. A secondary application of an in vivo anterior rectal wall dosimeter would be for target dose verification. The anterior rectal wall is generally contained by the Planning Target Volume (PTV) and therefore any dosimeter placed on the anterior rectal wall can be used as a surrogate for the PTV dose at the posterior region of the volume [48].

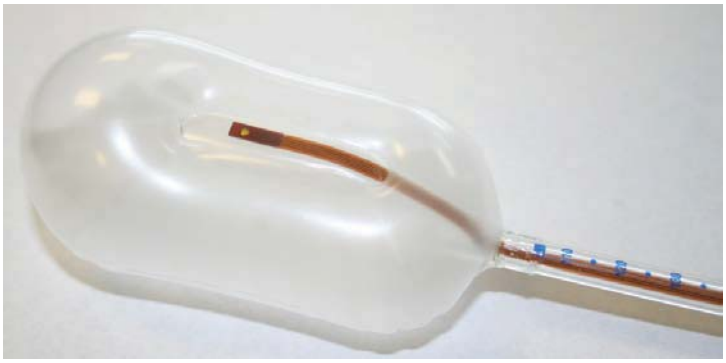

FIGURE 16. The dual MO*Skin*™ detectors placed in the outer lumen of the RadiaDyne (Houston, TX, USA) rectal balloon (Reproduce from [48]).

The rectal balloon with dual MO*Skin*™ detector was placed in a specially designed solid water phantom. A planning CT scan was taken of the phantom set up. The CT data was transferred to the Pinnacle treatment planning system (TPS) (Philips Medical Systems, Middleton, WI, USA) where contours of a hypothetical prostate, rectum (the balloon cavity), bladder and femoral heads were created. 3D conformal radiation therapy (CRT) and IMRT plans were created in the Pinnacle TPS. The dual MO*Skin*™ was visible on the CT scan and the planned dose to the detector was recorded for both treatment plans. Fig. 17 shows the real-time measured anterior rectal wall dose for (a) 3D CRT 7 field plan and (b) single fraction of an IMRT plan. The error bars are the 95% confidence interval of the average of three measurements.

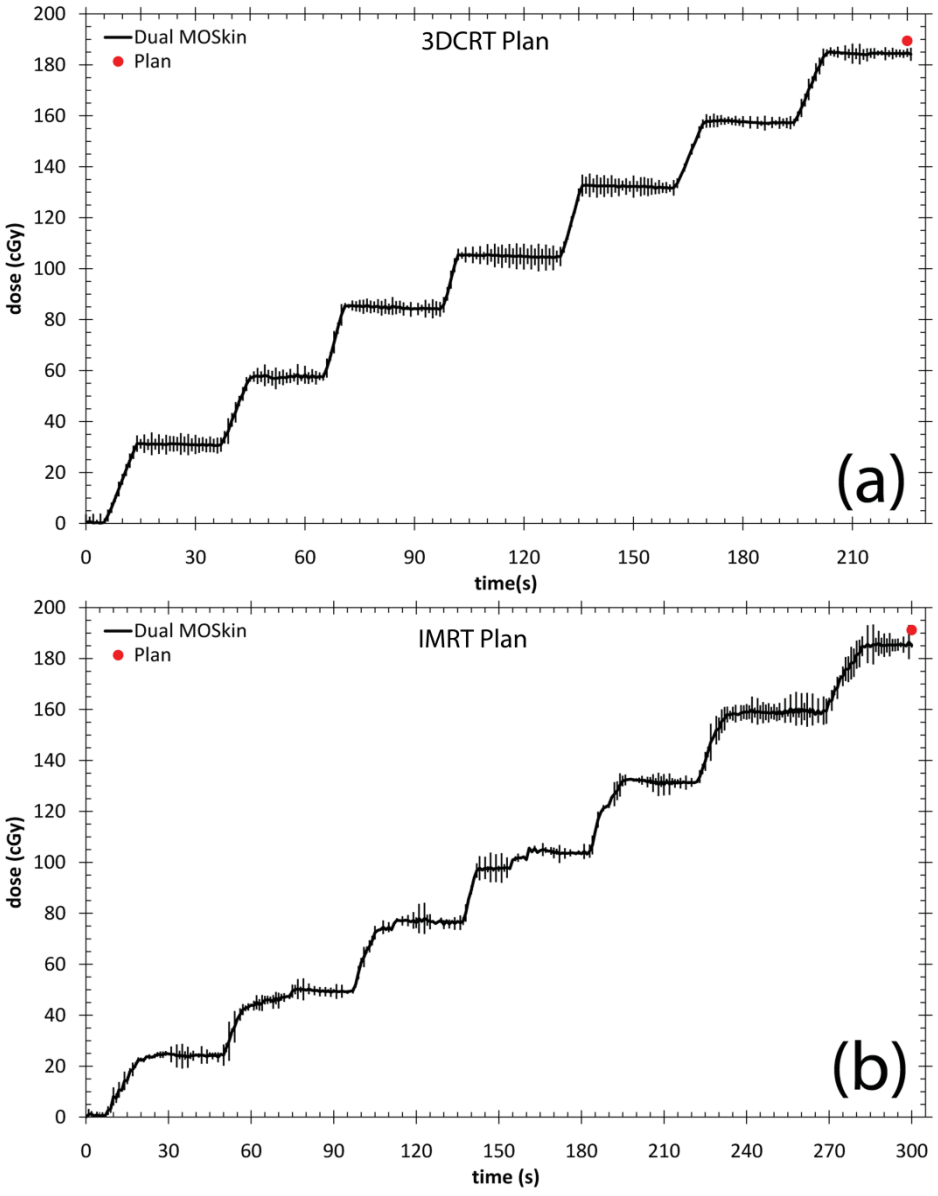

FIGURE 17. Real-time measured anterior rectal wall dose for (a) 3DCRT plan and (b) IMRT plan (Reproduce from [48]).

The difference in dose patterns between a) and b) is related to MLC leaf movement and is clearly reflected in the real-time MO*Skin*™ measurements. Measured and planned integral doses were in close agreement, confirming again that the MO*Skin*™ detector is a useful tool for real-time in vivo treatment delivery verification. More details can be found in [48].

The temperature dependence of the MO*Skin*^{TM} detector response, $V_{th}(T)$, is an important factor for in vivo dosimetry. This is particularly so when the temperature of the detector can change during the time between initial readout and readout after irradiation. This temperature dependence is dictated by the temperature dependence of the concentration and mobility of the charge carriers in the gate channel.

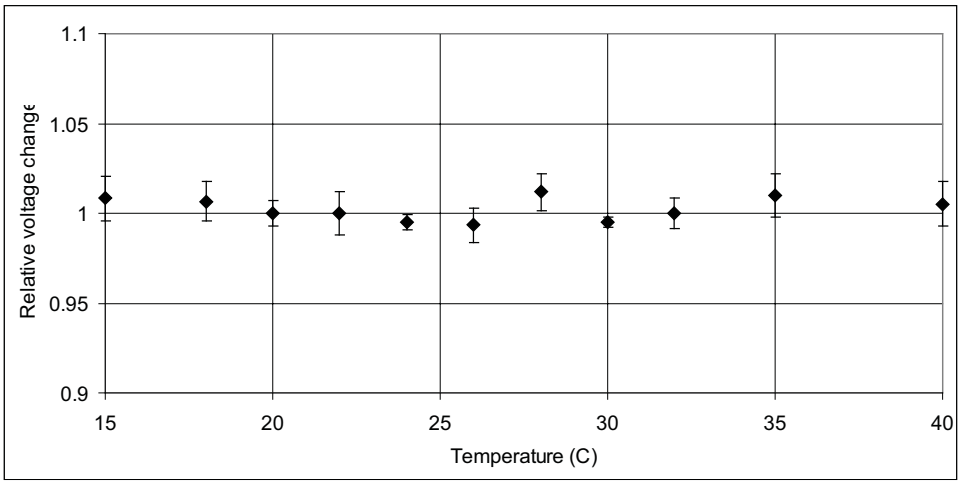

FIGURE 18. Temperature dependence of the response of the MOSFET detector irradiated under different temperatures. Picture is courtesy of M.Butson, ICCC, Australia.

Fig. 18 shows the relative dependence of the p-MOSFET (REM Oxford Ltd.) response when irradiated at different temperatures. The range of temperatures corresponded to that encountered for *in vivo* clinical conditions. The data was obtained with the CMRP MOSFET dosimetry system and presented in [72]. Similar results were demonstrated for an n-MOSFET over a temperature range of (-60 to +60)^{o}C [43]. The results demonstrate the temperature independence of sensitivity of the MOSFET detectors for clinically relevant temperatures. Thus, only a single calibration coefficient is required and changes in ambient temperature can be neglected when initial and final readout has been performed at the same temperature. If the latter does not hold, a temperature correction of V_{th} must be implemented or MOSFET should have built is temperature instability correction like mentioned above. For example, In the Best Medical MOSFET dosimetry systems, the dual MOSFET approach has been used to compensate for temperature instability of the threshold voltage [49].

SEMICONDUCTOR DOSIMETRY FOR DOSE EQUIVALENT IN CHARGED PARTICLE THERAPY

Microdosimetry

In conventional radiation therapy with electrons and photons, the absorbed dose and fractionation schedule are sufficient parameters for predicting tumor control. In charged particle therapy, neutron and binary therapies additional knowledge of the Radiobiological Efficiency (RBE) is important. In most of these therapies the RBE > 1 and in charged particle therapy is changing along the Bragg Peak (BP) or spread out Brag Peak (SOBP) due to a change in the LET of charged particles and the production of high LET products due to inelastic reactions. Charged particle therapy (proton and heavy ion) is very conformal and the discrete range of particles can be advantageous in sparing normal tissue. It is however accompanied by the production of neutrons in out-of-field areas that can lead to a risk in the production of second cancers. An estimation of the dose equivalent rather than absorbed dose is another important task of radiation dosimetry. The microdosimetry technique is based on a measure of the stochastic energy deposition events that occur on a cellular level, this is in contrast to the deterministic effect described by absorbed dose, and can be used for estimating the dose equivalent and RBE of therapeutic and mixed radiation fields. A detailed description of the microdosimetric approach and associated formalisms can be found in [73]

Semiconductor microdosimetry based on the representation of biological cells with an array of micron sized semiconductor sensitive volumes was introduced by us and described in [73, 74] and the references contained there.

In this paper the further progress on SOI semiconductor microdosimetry and examples of its application for dose equivalent and quality factor Q measurements in proton therapy is presented in brief.

The first generation of SOI microdosimeters was based on an array of adjacent right angular 30x30x10 μm^3 reverse biased p-n junctions (SVs). Shortcomings of this microdosimeter were the poorly defined charge collection volume and the localization of a single SV in comparison with a Tissue Equivalent Proportional Counter (TEPC) [75,76]. A new SV design has been proposed (see Fig. 19). This design aims to realize a 3D p-i-n diode with a well-defined cylindrical sensitive volume frequently used in TEPC. With this geometry, a better chord length variance is obtained when compared to an elongated rectangular geometry. A cylindrical volume supports a 1/r electrical field distribution which facilitates the collection of all deposited charge. Better localization of the SV outside of neighboring SVs has been achieved by the fabrication of mesa structures on SOI. A schematic of the new SV structure is shown in Figs. 20 (a) and (b). Fig 20 (c) shows array of mesa cylindrical SVs and a scanning electron microscope picture of a single mesa with connections. The fragment on Fig 20 (c) shows the way SVs are connected such that each SV is surrounded by another 4. Odd and even SVs are read out separately to realize the concept of regional microdosimetry in solid state microdosimetry. More details on the design of the second generation of SOI microdosimeters and their characterization can be found in [77-79]. The conversion of the silicon cylindrical SV geometry to water equivalent geometry can be achieved by simple scaling [80]. From this water or tissue equivalent microdosimetric spectra $y^2f(y)$ vs y can be found and finally the dose equivalent by combining the spectra with the defined ICRP quality factor Q(y) [73].

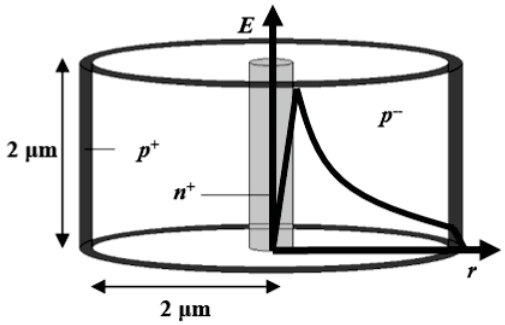

FIGURE 19. A schematic of the new 2nd Generation SOI SV (Reproduced from [78]).

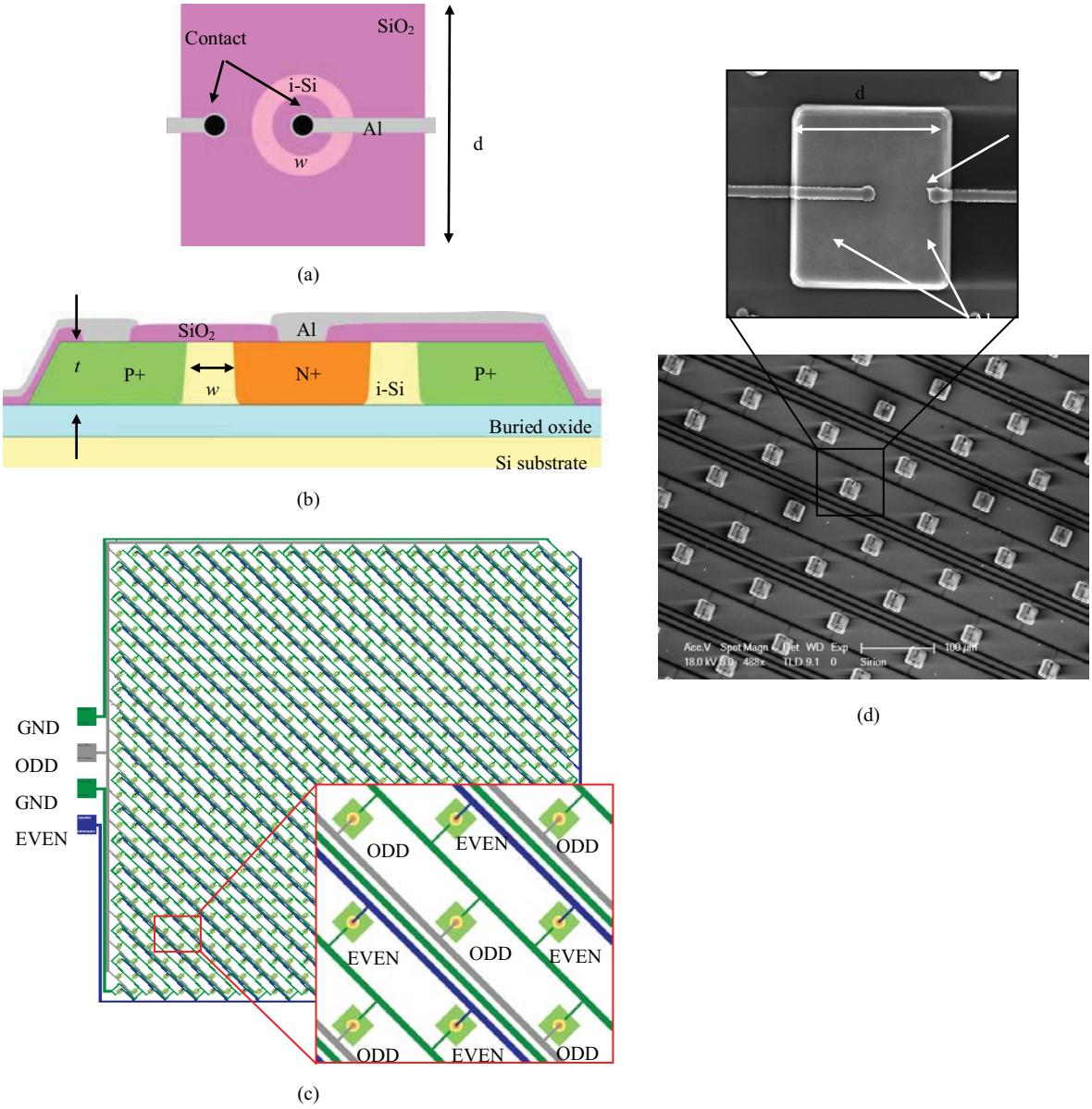

FIGURE 20. (a) Schematic top view of the cylindrical SV of SOI microdosimeter. (b) Schematic cross section of the cylindrical SV of SOI microdosimeter. (c) The microdosimeter array consists of array of cylindrical diodes. Individual diodes are connected odd-evenly in such a way that any single odd connected diode is surrounded by 4 identical even connected diodes.(d) electronic microscope picture of array of mesa SVs and single mesa SV as on a (b). (Reproduced from [78]).

In radiation therapy SOI microdosimetry has been applied to measure the dose equivalent outside of a primary proton beam. Both neutrons and scattered protons contribute to the dose equivalent in these regions. Passive beam delivery techniques provide a source of secondary neutrons due to the presence of beam modification devices such as scattering foils, modulator, aperture, and bolus [81]. Downstream of the Bragg peak the contribution to dose equivalent is from neutrons only. Active delivery techniques produce less neutrons out-of-field in comparison with passive delivery as has been demonstrated by Monte Carlo studies [82, 83]. Dose equivalents out-of-field using SOI microdosimeters were measured within a polystyrene phantom for different clinical scenarios at the Loma Linda University Medical Centre (LLUMC) and Massachusetts General Hospital (MGH) proton therapy facilities [84, 85]. Fig. 21 shows external field dose-equivalent and average quality factor values as a function of depth along the direction of the primary beam. The detector is situated at the height of the beam central axis for a patient-specific prostate configuration at a distance 5 cm from the field edge and for the solid brass beam block on the beam central axis. For the beam block, dose equivalent decreased from an initial value of 7.1 mSv/Gy at the phantom surface to

0.5 mSv/Gy at a depth of 33.5 cm. For the patient-specific configuration, dose equivalent decreased from an initial value of 5.5 to 2.4 mSv/Gy at 22.5-cm water equivalent depth (WED) normalized to 1 Gy absorbed dose delivered at the centre of the SOBP.

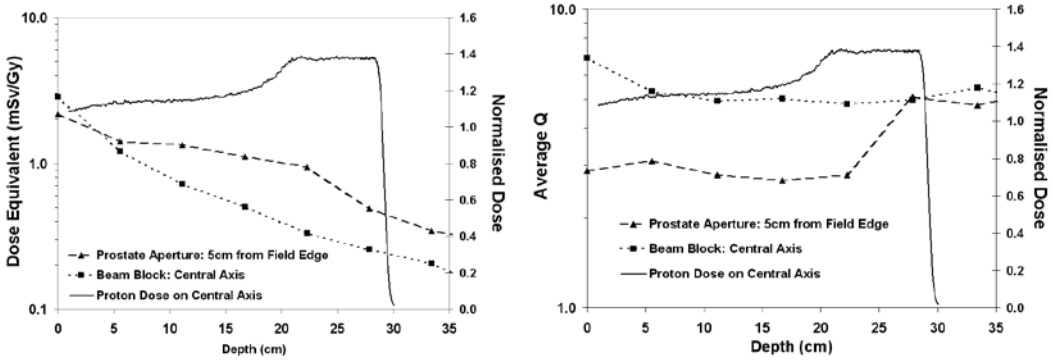

b)

FIGURE 21. Dose equivalent (a) and average quality factor (b) distributions as a function of depth within a homogeneous plexiglass phantom. Measurements completed using a patient specific aperture and bolus combination at 5cm from the field edge, and a solid brass beam block along the central axis. (Reproduced from [85]).

The average quality factor increased from 3 to 5 within the SOBP region of the patient specific treatment, while a decreasing quality factor was observed in the case of the beam block. This is because with depth the contribution to lateral dose equivalent is mostly from neutrons rather than high energy scattered protons. These neutrons are generating recoil protons with a higher LET than scattered protons. This is in good agreement with the quality factor along the central axis for the beam block and downstream of the SOBP where only neutrons are presented. More detailed information on the dose equivalent and Q-factors measured by SOI microdosimeters in out-of-field proton therapy can be found in [84,85]. An advantage of SOI microdosimetry is the small physical size of the detector SV in comparison with most TEPC and Bonner spheres. This allows measurement at points of interest close to the field edge and immediately behind the SOBP where critical organs may be located in many proton therapy scenarios.

ΔE-E Silicon Detectors in Proton Therapy dosimetry.

Monolithic silicon ΔE-E detectors have been found useful for dosimetry in proton therapy. Compared to a classical microdosimeter which provides one-dimensional information on the lineal energy spectra of primary and secondary charged particles, this detector system provides two-dimensional information on lineal energy and particle energy based on energy depositions collected in coincidence within the ΔE and E stages of the detector. This provides a unique signature for secondary or direct charged particles on a ΔE-E scatter plot.

A biological matrix can be formed by assigning each pixel on the scatter plot a RBE(α) value derived from V79 in vitro cell survival data in the low dose limit. The average RBE(α) can be presented as :

$$RBE(\alpha) = \frac{\sum_{i,j} N_{i,j} E_{i,j} RBE(\alpha)_{i,j}}{\sum_{i,j} N_{i,j} E_{i,j}} \quad (1)$$

where $N_{i,j}$ is the frequency of events for the cell ΔE_i , $(E+\Delta E)_j$ and $E_{i,j}$ is the energy deposited within the ΔE-E telescope for the cell ΔE_i , $(E+\Delta E)_j$. The resultant quantity RBE(α) is thus the dose-weighted average RBE in the low-dose limit for a given measured radiation field that is governed by the RBE(α) values used in the conversion matrix. This proposed approach to determining RBE in charged particle therapy is in addition to the classical regional microdosimetry approach linking experimental cell radiobiology closely to the detector response rather than only through the quality coefficient Q(y). This attempt is taking into account the track structure of the ion, i.e. two particles with the same Z^2/V^2 (Z- is a charge and V is a speed of particle) will have the same LET or lineal energy but will present at different locations on a ΔE-E scatter plot and as result possess different RBE(α).

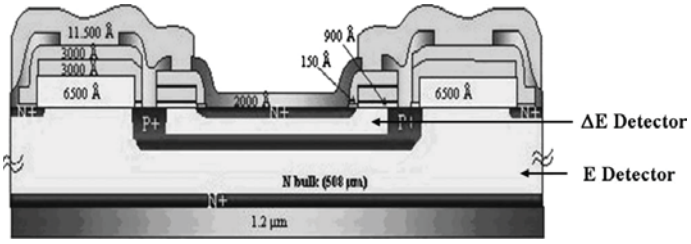

FIGURE 22. Monolithic ΔE-E detector comprised of ΔE 1.8μm thick -stage and E-500 μm stage. (Reproduced from [88]).

Fig. 22. shows a schematic of the ΔE-E monolithic detector which was developed by ST Microelectronics and Milano Polytechnic and has previously been described in detail [86]. In the ΔE-E detector a buried p+ layer was achieved via 2 MeV B implantation into the bulk of n- silicon. The detector had an effective surface area of 1x1 mm^2. During experiment the detector was housed in a specially designed PMMA probe within a PMMA phantom and irradiated with a 100 MeV proton beam. A custom made data aquistion system was used in read out. The probe was placed at different depths along the central axis of a pristine and SOBP as described in [87]. Fig. 23 shows an example of a ΔE-E scatter plot obtained at a depth of 7.5 cm corresponding to the distal edge of the 100 MeV proton Bragg peak. Fig 24 shows the RBE(α) matrix derived from published data on V79 cell survival data [87,88].

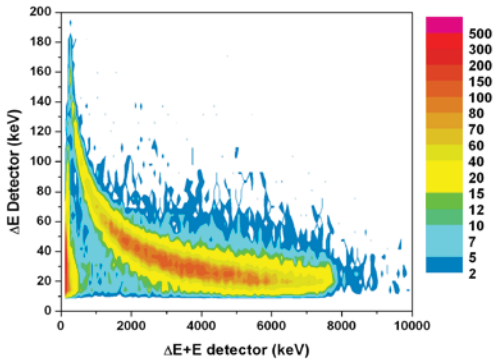

FIGURE 23. ΔE-E scatter plot at depth 7.5cm [88]

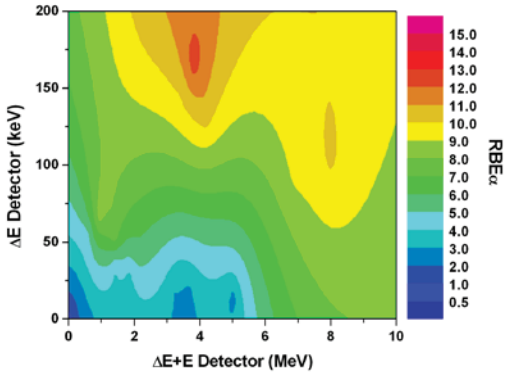

FIGURE 24. RBE(α) matrix. (Reproduced from [88]).

Fig 25 and 26 show the absorbed dose as measured by an ionization chamber in the PMMA phantom and the average RBE (α) change along the pristine and SOBP [87,88].

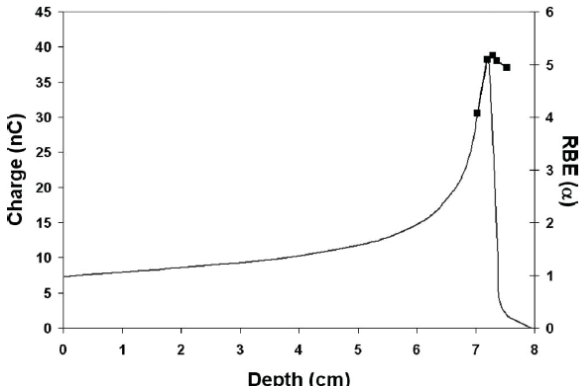

FIGURE 25. Total dose as measured by an ionization chamber and RBE(α) as measured by ΔE-E along a pristine BP (reproduce from [88]).

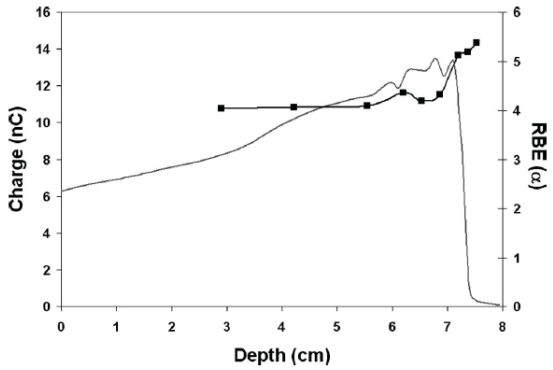

FIGURE 26. Total dose as measured by an ionization chamber and RBE(α) as measured by ΔE-E along a SOBP. (Reproduced from [88]).

The increase in RBE along the BP or SOBP was experimentally observed. The high spatial resolution of the detector made measurements possible, making it valuable for phantom measurements and QA applications in hadron therapy treatment planning. The difference in RBE (α) downstream of the BP and SOBP respectively may be attributed to the different neutron spectra present at the corresponding points due to the modulation wheel used to generate the SOBP.

As this method is based on actual radiobiological data, it can potentially be refined by including other in vitro and in vivo data for a range of cell lines, tissues, and clinical end points. Recently a monolithic ΔE-E detector was used for identifying the fragments produced on a 62 MeV/u ^{12}C ion beam [8]. With a range in PMMA of only 8 mm the spatial resolution of the ΔE-E detector was essential; measurements with a TEPC would not have been possible.

An advantage of semiconductor detectors for RBE and dose equivalent measurements in charged particle radiation therapy is their high spatial resolution. Measurements close to the field edge or at positions and detailed dosimetry along the BP and SOBP are easily obtained and would otherwise be impossible with a TEPC.

CONCLUSION

In this paper, current developments in semiconductor radiation detector technology for radiation therapy dosimetry and QA was presented. Silicon remains the main element of most clinical semiconductor dosimeters. The design of the single diode is continuing to improve. Passive diodes have been designed that allow charge collection from the total bulk volume, and consideration is being made into the packaging of single diodes to reduce the angular response and create effective detector depths relevant for skin dosimetry. For better phantom dosimetry on modern medical LINACs, sophisticated diode array dosimeters are being used. The recently developed ScandiDos Delta^4 (ScandiDose AB, Sweden), with two orthogonal diode array planes contained in a cylindrical phantom, and ArcCHECK, (Sun Nuclear Corporation, Melbourne, FL) with an isotropic arrangement of diodes embedded in a cylindrical phantom, combined with advanced read out algorithms allow comprehensive 3D dose verification QA in IMRT and VMAT.

A new trend in semiconductor dosimetry for QA involves multiple diode detectors on a silicon substrate, each read out individually using a specially designed multichannel ASIC. Such dosimeters allow high spatial resolution to be achieved. The Dose Magnifying Glass consists of a number of silicon strip detectors, it has high temporal resolution and provides a spatial resolution of 0.2mm which is otherwise impossible using a single diode array. The DMG provides a unique and important option for small field / real time phantom QA in SRS, IMRT and tomotherapy. It provides dosimetry options not possible using other detectors, including the EPID.

The MOSFET detector has been successfully used as a dosimeter in the clinic for over a decade. A recent advance in the MOSFET for clinical dosimetry is the MO*Skin*^{TM} . This detector utilizes special packaging technology that allows for reproducible skin dosimetry at a WED of 0.07 mm. MO*Skin*^{TM} detectors are used for in phantom QA, real time in vivo skin dosimetry of breast cancer patients, IMRT for NCP patients and can be placed on a rectal balloon for rectal wall dosimetry in prostate treatments. New packaging of MO*Skin*^{TM} detectors reduce the energy dependence of the detector response in comparison with the conventional epoxy bubble packed MOSFET detector and make the MO*Skin*^{TM} more suitable for HDR brachytherapy dosimetry. An important feature of this detector probe is that it is not affected by magnetic fields, making it suitable for real time QA in MRI guided radiotherapy.

Further development has been in integrated silicon dosimetry utilizing pixelated detectors. These detectors have a high spatial resolution and can be used for derivation of the relative RBE along the SOBP and in out-of-field regions. SOI microdosimeters with micron sized cylindrical sensitive volumes that better match a TEPC were developed and investigated. The SOI microdosimeter has been successfully used for dose equivalent measurements in out-of -field regions in proton therapy. A comparison of dose equivalent measures and associated risk of second cancer for different clinical scenarios was achieved. A new generation of microdosimeters will be produced based on Micro Electronic Mechanical Systems (MEMS) technology to produce micron sized free standing 3D cylindrical SVs with low capacitance [90].

Monolithic silicon ΔE-E detectors have traditionally been used in nuclear research for particle identification; recent work has applied them to RBE(α) derivation in proton therapy. Measurements were made along the Bragg peak and combined with known radiobiological cell data. The proposed silicon integrated detectors can be used for out-of-field neutron dosimetry on medical LINACs similar to proton therapy.

Further semiconductor clinical dosimetry has been in a progress which was not included in this paper. The pixilated silicon detector MEDIPIX has been successfully used for fast 3D dosimetric imaging with spatial resolution 55 microns of eye plaques with I-125 seeds and Ru-106, details can be found in [91]. The advantage of microelectronics was recently realized in new miniature Si special diode detectors, allowing 5 μm spatial resolution in real time dose verification for in-phantom QA on MRT beam array [92]. The progress in semiconductor detector technology clearly demonstrates the future such detectors have for QA in clinical dosimetry with high spatial resolution, real time dosimetric imaging possible.

ACKNOWLEDGEMENT

Many collaborators took part in this development. Author would like to thanks all staff and PhD students of Centre for Medical Radiation Physics who were involved in semiconductor dosimetry development presented in this review. Thanks to Australian collaborators on microdosimetry from SNF UNSW and ANSTO detector group. Thank you to our international collaborators from LLUMC proton therapy facility, Wisconsin University hospital in the USA , Milano Politechnik , Italy and Radiation Oncology Department, Sun Yat-Sen University Cancer Center, Guangzhou , China. Thank you to staff of microelectronic foundry SPA BIT for fabrications of designed at CMRP detectors. Special thanks to Dean Cutajar and my PhD students Jeannie Wong, Amy Ziebell, CMRP, for helping with manuscript preparation and editing

REFERENCES

1. P.Bradley, A.B.Rosenfeld, M.Zaider ,*Solid state microdosimetry*, Nucl.Instr.Meth. in Phys. Research B, **184**, 135-157, (2001)
2. A.B.Rosenfeld, *Electronic dosimetry in radiation therapy* , Radiation Measurements , **41**, 134-153, (2007)
3. AAPM Comprehensive QA for radiation oncology, Task Group 40, Radiation Therapy Committee, 1993.
4. S. M. Zee *Physics of semiconductor devices*, 2nd edition, John Wiley & Sons, 1981.
5. J. Shi, W. E. Simon, T. C. Zhu, *Modelling the instantaneous dose rate dependence of radiation diode detectors*, Med.Phys. **30**, 2509-2519, (2003).
6. D. Marre, G. Marinello, *Comparison of p-type commercial electron diodes for in-vivo dosimetry*, Med. Phys. **31**, 50-56, (2004).

7. A. Jursinic, *Implementation of an in-vivo diode dosimetry program and changes in diode characteristics over 4-years clinical history*, Med. Phys. **28**, 1718-1726, (2001).
8. A.S.Saini, T.C.Zhu, *Temperature dependence of commercially available diode detectors*, Med.Phys. **29**, 622-630, (2002).
9. D. Létourneau, M. Gulam, D. Yan, M. Oldham and J. W. Wong, *Evaluation of a 2D diode array for IMRT quality assurance*, Radiother. Oncol. **70(2)**, 199-206 (2004).
10. P. A. Jursinic, B. A. Nelms, *2-D diode array and analysis software for verification of intensity modulated radiation therapy delivery,* Med Phys. **30,** 870–879, (2003).
11. P. A. Jursinic, R. Sharma, and J. Reuter, *MapCHECK used for rotational IMRT measurements: Step-and-shoot, Tomotherapy, RapidArc*, Med. Phys. **37**, 2837-2846, (2010).
12. J. L. Bedford, Y. K. Lee, P. Wai, C. P. South and A. P. Warrington, *Evaluation of the Delta4 phantom for IMRT and VMAT verification*, Phys. Med. Biol. **54 (9)**, N167-N176 (2009).
13. V. Feygelman, K. Forster, D. Opp, and G. Nilsson, *Evaluation of a biplanar diode array dosimeter for quality assurance of step-and-shoot,* IMRT Journal of Applied Clinical Medical Physics, **10**, N4 , 64-78, (2009).
14. S. Korreman, J. Medin, F. Kjaer-Kristoffersen, *Dosimetric verification of treatment of RapidArc treatment delivery*, Acta Oncologica, **48**, 185-191, (2009).
15. G. Yan, B. Lu, J. Kozelka, C. Liu and J. G. Li, *Calibration of novel four-dimensional diode array*, Med. Phys. **37**, 108-115, (2010).
16. K. T. Welsh, L. E. Reinstein, *The thermal characteristics of different diodes on in-vivo patient dosimetry*, Med.Phys. **28**, 844-849, (2001).
17. P. Jursinic, *Angular dependence of dose sensitivity of surface diodes,* Med Phys **36 (6)**, 2165, (2009).
18. D. Menichellia, M. Bruzzi, M. Bucciolini et.al, *Design and development of a silicon segmented detector for 2D dose measurements in radiotherapy*, Nuclear Instruments and Methods in Physics Research A **583** 109–113,(2007).
19. M. Caccia, M. Alemi, C. Bianchi, A. Bulgheroni, C. Cappellini, W. Conte L, Kucewicz, M. Prest, E. Vallazza and C. Sampietro, *Imaging of [beta] particle sources used in medical applications with position sensitive Silicon sensors*. Nucl. Instr. and Meth. in Physics Research Section A:, **525(1-2)**, 294-297, (2004).
20. E. Pappas, T. G. Maris, F. Zacharopoulou, A. Papadakis, S. Manolopoulos, S. Green and C. Wojnecki, *Small SRS photon field profile dosimetry performed using a PinPoint air ion chamber, a diamond detector, a novel silicon-diode array (DOSI), and polymer gel dosimetry. Analysis and intercomparison*. Med. Phys., **35(10)**, 4640-4648. (2008).
21. S. Manolopoulos, C. Wojnecki, R. Hugtenburg, M. J. Sidek, G. Chalmers, G. Heyes and S. Green, *Small field measurements with a novel silicon position sensitive diode array*. Phys. Med. Biol., **54(3)**, 485-495, (2009).
22. G. C. Bonazzola, R. Cirio, M. Donetti, F. Marchetto, G. Mazza, C. Peroni and A. Zampieri, *Performances of a VLSI wide dynamic range current-to-frequency converter for strip ionization chambers*. Nuclear Instruments and Methods in Physics Research Section A: Accelerators, Spectrometers, Detectors and Associated Equipment, **405(1)**, 111-120, (1998).
23. R. Cirio, F. Bourhaleb, P. G. Degiorgis, M. Donetti, F. Marchetto, M. Marletti, G. Mazza, C. Peroni, E. Rizzi and C. Sanzfreire, *Radiation damage studies of a recycling integrator VLSI chip for dosimetry and control of therapeutical beams*. Nuclear Instruments and Methods in Physics Research Section A: Accelerators, Spectrometers, Detectors and Associated Equipment, **482(3)**, 752-760. (2002).
24. A. La Rosa, G. Mazza, M. Donetti, F. Marchetto, L. Luetto, A. Attili, F. Bourhaleb, R. Cirio, M. A. Garella, S. Giordanengo, N. Givehchi, S. Iliescu, J. Pardo, A. Pecka, C. Peroni and G. Pittà, *Design and test of a 64-channel charge measurement ASIC developed in CMOS 0.35 μm technology*. Nuclear Instruments and Methods in Physics Research Section A: Accelerators, Spectrometers, Detectors and Associated Equipment, **583(2-3)**, 461-468, (2007).
25. Brusasco C, Cattai A, Cirio R, Dellacasa G, Donetti M, Isoardi P, Marchetto F, Peroni C, Rolando V, Ruspa M, Solano A & Zambernardi C, *Strip ionization chambers as 3-D detector for hadron therapy*. Nuclear Instruments and Methods in Physics Research Section A: Accelerators, Spectrometers, Detectors and Associated Equipment, **389(3)**, 499-512, (1997).
26. La Rosa A, Garella M A, Bourhaleb F, Cirio R, Donetti M, Giordanengo S, Givehchi N, Marchetto F, Martin F, Meyroneinc S, Peroni C & Pittà G, *A pixel ionization chamber used as beam monitor at the Institut Curie--Centre de Protontherapie de Orsay (CPO)*. Nuclear Instruments and Methods in Physics Research Section A: Accelerators, Spectrometers, Detectors and Associated Equipment, **565(2)**, 833-840, (2006).
27. La Rosa A, Donetti M, Borri M, Rivero F, Attili A, Bourhaleb F, Cirio R, Garella M A, Giordanengo S, Givehchi N, Mazza G, Marchetto F, Pardo J, Pecka A & Peroni C, *Characterization of a front-end electronics for the monitoring and control of hadrontherapy beams*. Nuclear Instruments and Methods in Physics Research Section A: Accelerators, Spectrometers, Detectors and Associated Equipment, **586(2)**, 270-275, (2008).
28. Wong J H D, Carolan M, Lerch M L F, Petasecca M, Khanna S, Perevertaylo V L, Metcalfe P & Rosenfeld A B, *A silicon strip detector dose magnifying glass for IMRT dosimetry*. Med. Phys., **37(2)**, 427-439, (2010a).
29. Meyer P, Regal R, Jung M, Siffert P, Mertz L & Constantinesco A, *Feasibility of a semiconductor dosimeter to monitor skin dose in interventional radiology*. Med. Phys., **28(10)**, 2002-2006, (2001).
30. Poppe B, Djouguela A, Blechschmidt A, Willborn K, Ruhmann A & Harder D, *Spatial resolution of 2D ionization chamber arrays for IMRT dose verification: single-detector size and sampling step width*. Phys. Med. Biol., **52(10)**, 2921-2935, (2007).
31. Grosu a-L, Kneschaurek P & Schlegel W, *Stereotactic Radiotherapy/Radiosurgery*. IN SCHLEGEL W, BORTFELD T & GROSU A-L (Eds.) New Technologies in Radiation Oncology. Berlin Heidelberg, Springer-Verlag 2006.

32. García-Vicente F, Béjar M J, Pérez L & Torres J J, *Clinical impact of the detector size effect in 3D-CRT. Radiotherapy and oncology : journal of the European Society for Therapeutic Radiology and Oncology*, **74(3)**, 315-322, (2005).
33. Laub W U & Wong T (2003) The volume effect of detectors in the dosimetry of small fields used in IMRT. Med. Phys., 30(3), 341-347.
34. Wong J H D, Knittel T, Downes S, Carolan M, Lerch M, Petasecca M, Perevertaylo V L, Metcalfe P, Jackson M & Rosenfeld a B The use of a Silicon Strip Detector Dose Magnifying Glass in Stereotactic Radiotherapy QA and Dosimetry. Med. Phys., (2011) (in press).
35. Mackie T R, History of tomotherapy. Phys. Med. Biol., **51(13)**, R427, (2006).
36. Balog J & Soisson E, *Helical Tomotherapy Quality Assurance*. Int. J. Radiat. Oncol. Biol. Phys., **71**(1, Supplement 1), S113-S117, (2008).
37. Fenwick J D, Tomé W A, Jaradat H A, Hui S K, James J A, Balog J P, Desouza C N, Lucas D B, Olivera G H, Mackie T R & Paliwal B R, *Quality assurance of a helical tomotherapy machine*. Phys. Med. Biol., **49(13)**, 2933-2953, (2004).
38. Balog J, Olivera G & Kapatoes J, *Clinical helical tomotherapy commissioning dosimetry*. Med. Phys., 30(12), 3097-3106, (2003b).
39. Balog J, Mackie T R, Pearson D, Hui S, Paliwal B & Jeraj R, *Benchmarking beam alignment for a clinical helical tomotherapy device*. Med. Phys*.,* 30(6)**,** 1118-1127, (2003a).
40. Wong J H D, Hardcastle N, Bayliss A, Tolakanahalli R, Tomé W A, Lerch M L F, Petasecca M, Metcalfe P, Carolan M & Rosenfeld A B, *Independent quality assurance of a helical tomotherapy machine using the dose magnifying glass*. Med. Phys., (2011). (in press)
41. Holmes-Siedle, *The Space Charge Dosimeter,* Nucl. Inst. Meth,, **121**, 169-179, (1974).
42. Freeman, R., Holmes-Siedle, A., A Simple Model for Predicting Radiation Effects in MOS Devices, IEEE Trans. Nucl. Sci., NS-25-6,1216-1225, (1978).
43. P.G.Litovchenko, L.I.Barabash, A.B.Rosenfeld et. al. "MOS structure for emergency gamma and proton dosimetry" , Rad. Prot. Dos.33, N1/4, 179-182, 1990.
44. Rosenfeld, A.B. (*invited paper*) "MOSFET dosimetry in modern radiation oncology modalities", *Rad. Prot.Dosim*, **101**, N1/4, 393-398, 2002.
45. A.Holmes-Siedle, L. Adams Handbook of radiation effects**,** second edition **,** Oxford University press, 2002.
46. Rosenfeld, A.B., Lerch, M.L.F., et al, Feasibility Study of On-line, High Spatial Resolution MOSFET Dosimetry in Static and Pulsed X-ray Radiation Fields, IEEE Trans. Nucl. Sci., NS-48-N6, (2001).
47. Zhen-Yu Qi, Xiao-Wu Deng , Shao-Min Huang, Li Zhang, Zhi-Chun He, X. Allen Li Ian Kwan, Michael Lerch , Dean Cutajar, Peter Metcalfe, **Anatoly Rosenfeld** "In vivo verification of surface and superficial dose for head and neck treatments using intensity-modulated techniques" , Med. Phys **36**(1), 59 – 70 (2009).
48. Nicholas Hardcastle, Dean L. Cutajar, Peter E. Metcalfe, Michael L. F. Lerch, Vladimir L. Perevertaylo, Wolfgang A. Tomé, Anatoly B. Rosenfeld "*In vivo* real-time rectal wall dosimetry for prostate radiotherapy", Phys.Med.Biol. 55, 3859-3871, 2010.
49. Soubra, M., Cygler, J., Mackay, G., Evaluation of a Dual bias Dual Metal Oxide-Silicon Semiconductor Field Transistor Detector as Radiation Dosimeter, Med. Phys., 21-4, 567-572, 1994.
50. Halvorsen, P.H., *Dosimetric evaluation of a new MOSFET in vivo dosimeter*, Med.Phys., 31(2), 110-117, (2005).
51. Quach, K.Y., Morales, J., Butson, M.J., Rosenfeld, A.B., Metcalfe, P.E., Measurements of Radiotherapy X-ray Skin Dose on a Chest Wall Phantom, Med. Phys., 27-7, 1676-1680, (2000).
52. Cheung, T., Butson, M.J., Yu, P.K.N. *Effect of temperature variation on MOSFET dosimetry*, Phys. Med.Biol., 49, 191-196, (2004).
53. T.Kron, A.Rosenfeld, M.Lerch, *Measurements in radiotherapy beams using on-line MOSFET detectors*, Rad.Prot.Dos., 101, N1/4, 445-448, (2002).
54. Butson, M., Cheung, T., Yu, P.K.N., *Peripheral dose measurement with a MOSFET detector*., Applied Radiation and Isotopes, 62, 631-634, (2005).
55. Rosenfeld, A.B. (*invited paper*), *MOSFET dosimetry in modern radiation oncology modalities*, Rad. Prot.Dosim, **101**, N1/4, 393-398, (2002).
56. Valery Oliver Zilio, Om Parkash, Youri Popowski, Anatoly Rosenfeld, Rakesh Chawla, *Absolute depth-does-rate measurements for an Ir-192 HDR brachytherapy source in water using MOSFET detectors,* Med.Phys., **33**(6), 1532-1539, (2006).
57. Zhen-Yu Qi , Xiao-Wu Deng, Shao-Min Huang, Jie Lu , Michael Lerch , Dean Cutajar , Anatoly Rosenfeld, *Verification of the plan dosimetry for high dose rate brachytherapy using MOSFET detectors*, Med. Phys., **34**,(6), 2007-2013, (2007).
58. Rosenfeld, A.B., Kaplan, G.I., Allen, B.A., Dilmanian, A., Kron, T., Holmes-Siedle, A., *MOSFET Dosimetry of X-ray Microbeams*, IEEE Trans. on Nucl Sci. , NS-46, N6, 1774-1780, (1999).
59. E.Brauer-Krish, A.Bravin, M.Lerch, A.Rosenfeld, J.Stepanek, M.Di.Michiel, J.A.Laissue, *MOSFET dosimetry for Microbeam radiation therapy at the European Synchrotron Radiation Facility*, Med.Phys., 31(3), 609-615, (2004).
60. Rosenfeld, A. B., Erik A. Siegbahn, Elke Brauer-Krish, Andrew Holmes-Siedle, Michael L.F.Lerch, Alberto Bravin, Iwan M. Cornelius, George J. Takacs, Nirmal Painuly, Heidi Nettelback, Tomas Kron, *Edge on Face-to-Face (EOFF) MOSFET for Synchrotron Microbeam Dosimetry: MC modeling*, IEEE Trans on Nucl. Sci., NS-52, N6 , December, (2005).
61. A. Siegbahn, E. Bräuer-Krisch , A. Bravin, H. Nettelbeck, M. L. F. Lerch and A. B. Rosenfeld, *MOSFET dosimetry with high spatial resolution in intense synchrotron-generated x-ray microbeams***,** Med Phys**,** 36(4), 1128-1137, (2009).

62. Rosenfeld, A.B., Carolan, M.G., Allen, B.J., et al, *MOSFET Dosimeters: role of encapsulation in mixed gamma-neutron and megavoltage X-ray fields*, IEEE Trans. on Nucl. Sci., NS-42, N6, 1870-1877, (1995).
63. Rosenfeld, A., Kaplan, G., Carolan, M., B. Allen, Maughan, R., Yudelev, M., Cota, C., and. Coderre, J., *Simultaneous Macro and Micro Dosimetry with MOSFETs*, IEEE Trans. Nucl. Sci., vol. 43, pp. 2693-2700, (1996).
64. G.Kaplan, A.B.Rosenfeld, B.Allen, J.A.Coderre, H.B.Liu, *Fission converter and MOSFET study of thermal neutron flux distribution in an epithermal neutron therapy beam*, Med.Phys.,26(9), 1989-1994, (1999).
65. ICRP 1975.
66. Butson, M.J., Rozenfeld, A.B., Mathur, J.N., Carolan, M., Wong, T.P., Metcalfe, P.E., *A New Radiotherapy Surface Dose Detector: The MOSFET*, Med. Phys., *23-5,* 655-658, (1996).
67. Ramani, R., Russell, S., O'Brien, P., *Clinical Dosimetry using MOSFETs*, Int. J. Radiation Oncology Biol. Phys., 37-4, 959-964, (1997).
68. Zhen-Yu Qi, Xiao-Wu Deng, Shao-Min Huang, Xiao-Yan Huang, Zhi-Chun He, Tomas Kron Michael Lerch, Peter Metcalfe, Anatoly Rosenfeld, *Real-Time In Vivo Dose Verification for Serial Tomotherapy of Head and Neck Patients* , IJROPB, (2010) (accepted).
69. Zhenyu Qi "MOSFET Dosimetry in HDR Brachytherapy and IMRT for Nasopharyngeal Carcinoma", PhD thesis , University of Wollongong, 2011
70. Chung H, Jin H, Dempsey JF, Liu C, Palta J, Suh T-S, Kim S, Evaluation of surface and build-up region dose for intensity-modulated radiation therapy in head and neck cancer. Med Phys. 32(8): 2682-2689 (2005).
71. I. S. Kwan, D. Wilkinson, D. Cutajar, M. Lerch, , Y.Wong, J.Bucci, V.Perevertaylo A. B. Rosenfeld, *The effect of rectal heterogeneity on wall dose in High Dose-Rate brachytherapy*, Med. Phys **36**(1), 224 – 232 (2009).
72. Cheung, T., Butson, M.J., Yu, P.K.N., *Effect of temperature variation on MOSFET dosimetry*, Phys. Med. Biol., 49, 191-196, (2004).
73. H.H. Rossi and M. Zaider, *Microdosimetry and its Applications*. London: Springer, 1996
74. P. D. Bradley, A. B. Rosenfeld, and M. Zaider, *Solid state Microdosimetry*," *Nucl. Instrum. Methods Phys. Res. B*, vol. B184, pp. 135–157, (2001).
75. P.D. Bradley, A.B. Rosenfeld, K.K. Lee, D.N. Jamieson, G. Heiser, S.Satoh, *Charge Collection and Radiation Hardness of a SOI Microdosimeter for Medical and Space Applications*, IEEE Trans. onNucl. Science, vol. 45, no. 6 (1998).
76. I. Cornelius, R. Siegele, A.B. Rosenfeld, D.D. Cohen, *Ion Beam Induced Charge Characterisation of a Silicon Microdosimeter Using a Heavy Ion Microprobe*, Nucl. Instr. and Meth. in Phys. Res. B, vol. 190 pp. 335-338 (2002).
77. A.L.Ziebell, W.H.Lim, M.I.Reinhard, I.Cornelius, D.A.Prokopovich, R.Siegele, A.S.Dzurak, A.B.Rosenfeld, *Cylindrical Silicon-on-Insulator Microdosimeter: Charge Collection Characteristics*, IEEE Trans on Nucl Sci., NS- 55, 3414 – 3420, (2008).
78. W.H. Lim, A.L. Ziebell, I. Cornelius, M.I. Reinhard, D.A. Prokopovich, A.S. Dzurak and A.B. Rosenfeld, *Cylindrical Silicon-on-Insulator Microdosimeter: Design , Fabrication and TCAD modelling*, IEEE Trans on Nucl. Sci., NS-56, issue 2, 424-428, (2009).
79. N.S. Lai, W.H. Lim, A.L. Ziebell, M.I. Reinhard, A.B. Rosenfeld, A.S. Dzurak, *Development and Fabrication of Cylindrical Silicon-on-Insulator Microdosimeter Arrays*", IEEE Trans on Nucl. Sci. ,NS-56 , 1637-1641, (2009).
80. S. Guatelli, M.I. Reinhard, D. A. Prokopovich, B. Mascialino, A. S. Dzurak, M. Zaider and A. B. Rosenfeld, *Tissue equivalence correction in silicon microdosimetry for protons characteristic of the LEO space environment*, IEEE Trans. on Nucl . Sci , NS -55, 3407-3413, (2008).
81. E. J. Hall, *Intensity-modulated radiation therapy, protons, and the risk of second cancers*, Int. J. Radiat. Oncol. Biol. Phys. **65**, 1–7, (2006).
82. Xu XG, Bednarz B, Paganetti H. *A review of dosimetry studies on external-beam radiation treatment with respect to second cancer induction*. Phys Med Biol, **53**, R193– R241, (2008).
83. Ben Clasie, Andrew Wroe, Hanne Kooy, Nicolas Depauw, Jay Flanz, Harald Paganetti , Anatoly Rosenfeld, *Assessment of out-of-field absorbed dose and equivalent dose in proton fields*, Med. Phys.,**37**(1),311-321, (2010).
84. A. Wroe, A.Rosenfeld, and R. Schulte, *Measured Out-Of-Field Dose Equivalents Delivered by Proton Therapy of Prostate Cancer,* Med. Physics, **34**(9), 3449-3455, (2007).
85. Andrew Wroe , Ben Clasie , Hanne Kooy , Jay Flanz , Reinhard Schulte, Anatoly Rosenfeld, *Out-Of-Field Dose Equivalents Delivered by Passively Scattered Therapeutic Proton Beams for Clinically Relevant Field Configurations*, Int. Journal Rad. Oncol. Phys. and Biol. (IJOROPB), **73**, 306-313, (2009).
86. S. Agosteo, P. G. Fallica, A. Fazzi et al., *A feasibility study of a solid-state microdosimeter*, Applied Radiation and Isotopes **63** (5-6), 529 (2005).
87. A.Wroe, Development in microdosimetry and nanodosimetry for space and therapeutic applications, PhD Thesis, University of Wollongong, (2007)
88. A.Wroe, R. Schulte, A. Fazzi, A. Pola, S. Agosteo, A.B.Rosenfeld, *RBE estimation of proton radiation fields using a ΔE-E telescope* ,Med. Phys., 36(10):4486-94, (2009).
89. A. Fazzi, A. Pola, M. V. Introini et al., *Fragment identification in a 62 MeV/u ^{12}C Ion Beam*, Radiation Measurements (2011), in press.
90. C. Fleta, D. Pennicard, R. Bates, C. Parkes et al. G. Pellegrini, M. Lozano, V. Wright, M. Boscardin, G.-F. Dalla Betta, C. Piemonte, A. Pozza, S. Ronchin and N. Zorzi, *Simulation and test of 3D silicon radiation detectors*, Nucl. Instr. Meth,, 579, Issue 2 , 642-647, (2007).

91.M. Weaver, J. Green, M. Petasecca, A. Rosenfeld et al ,*Three-dimensional dosimetry imaging of I-125 plaque for eye cancer treatment,* Nucl. Instr. Meth. A. accepted http://dx.doi.org/10.1016/j.nima.2010.06.187
92. M.L.F. Lerch, M. Petasecca, V.L. Perevertaylo, A.B. Rosenfeld, *Dosimetry of intensive synchrotron microbeams*, Radiation Measurements, (2011) in press